Mathematisches Forschungsinstitut Oberwolfach

Transport and Scale Interactions in Geophysical Flows

Organized by
Christian L. E. Franzke, Busan
Marcel Oliver, Ingolstadt
Jens Rademacher, Hamburg
Irina Rypina, Woods Hole

16 July – 21 July 2023

ABSTRACT. This interdisciplinary workshop brought together researchers working on different aspects of transport and scale interactions across the spectrum of geophysical fluid dynamics: geometry and computation of transport and exchange processes in geophysical flows, Lagrangian coherent structures, (geo-strophic) turbulence, nonlinear waves and coherent structures in the Eulerian description of fluids, and stochastic methods in multiscale systems. Each of these topics have their own vibrant communities as well as well-established and emerging connections. This meeting aimed to bridge across the entire span of topics from a dynamical systems perspective, and to connect classical approaches with new developments in data-driven modeling and stochastic modeling.

Introduction by the Organizers

This interdisciplinary workshop concerned various aspects of transport and scale interactions in geophysical fluid dynamics through the lens of dynamical systems methods. There were 44 participants present in Oberwolfach and up to 8 online.

Geophysical fluid flow is fundamentally intertwined with transport in different ways. Passive transport of buoyancy, tracers, and solid particles is one of the more visible aspects. Other transported quantities are "active", interacting with themselves, other scalars, or the flow. In geophysical flows, the arguably most prominent active scalar is the potential vorticity which dominates the dynamics of rotating stratified flow. It connects transport to geostrophic turbulence, its

characteristic feature being the cascade of energy to large scales, a process which favors the emergence of large-scale, coherent structures which, in turn, determine mixing and transport of other Lagrangian quantities.

The range of problems include the analysis of scale interaction, the parametrization of unresolvable scales and unresolvable physics in computational models through surrogate models or consistent closures, emergence and dynamics of coherent structures, the characterization of coherent structures as nonlinear waves as well as through data-driven methods, and their interaction with secondary processes such as solid particles and complex bio-geochemistry.

Particular emphasis was given to approaches that bridge between subfields, exemplified by the emergence of Eulerian stochastic PDEs from Lagrangian particle dynamics, the connection between asymptotic and data-driven methods in weakly coupled systems and the emerging use of transfer operator techniques for black-box modeling of dynamical systems. Key aspects were thus:

- Lagrangian Transport in Geophysical Fluid Flows
- Lagrangian Coherent Structures and Barriers
- Turbulence
- PDEs, nonlinear waves and coherent velocity structures
- Transport under Uncertainty

The contributions in this report reflect this melange and were augmented by discussion sessions that prompted subsequent individual intense discussions. Notably, a reappearing subject of discussion concerned the practice and boundaries of machine learning in this field. We also felt that the poster pitches before dinner and poster sessions after dinner worked rather well and fostered further interactions; all posters were present for the duration of the workshop.

We believe the workshop has strengthened existing and explored new connections between the above five topic areas and their communities.

The workshop organizers thank in particular the conference video assistants Paul Holst and Marc Tiofack for managing the partial hybrid nature and online as well as on-site technology, and Anton Kutsenko for collecting the abstracts for this report, and putting it together.

We also thank the MFO the staff for the wonderful hospitality.

Workshop: Transport and Scale Interactions in Geophysical Flows

Table of Contents

Abstracts

Parameterization of mesoscale eddies via kinetic energy backscatter (deterministic and stochastic options)

EKATERINA BAGAEVA

One way to overcome limitations in ocean resolution is by parametrizing physical processes. However, traditional parameterization methods applied to the mesoscale range processes on eddy-permitting mesh resolutions, known as viscous momentum closure, result in over-dissipation of eddy kinetic energy. To address this issue, the viscous closure has an energy backscatter that returns energy back to the system. We work with the dynamic energy backscatter that is based on the amount of unresolved kinetic energy (UKE). Our study suggests that including the advection of UKE can consider the effects of nonlocality on the subgrid. Additionally, we recommend incorporating a stochastic element into the subgrid energy equation to account for variability, which is not present in a deterministic approach.

This approach has been shown to increase eddy activity and improve flow characteristics, including mean vertical profiles, KE and dissipation spectra, and sea surface height. Our implementations are tested on two intermediate complexity setups of the global ocean model FESOM2 (the Finite-volume Sea ice-Ocean Model), which include an idealized channel setup and a double-gyre setup.

Extending stochastic sensitivity: probabilistically quantifying the impact of subgrid scales on Lagrangian transport

SANJEEVA BALASURIYA

(joint work with Liam Blake, John Maclean)

When assessing transport in geophysical flows, an important consideration is that the unsteady Eulerian velocity data is usually only available on a spatio-temporal grid. Consequently, any inferred transport from such data will inevitably not have information on subgrid scales (the so-called "stochastic parametrization" problem [2]), or of effects occurring on time-scales smaller than available. This means that simply using the velocity data as given in assessing transport will lead to errors, as the data would need to be interpolated to the subgrid scale when computing the Lagrangian motion of fluid parcels or tracers. In essence, one is using a potentially unjustified extension of the gridded Eulerian velocity field, without taking into consideration the fact that this extension must have an uncertainty associated with it. Indeed, observed or measured Eulerian velocity data of geophysical flows typically has many different types of uncertainties:

(1) The *subgrid-scale uncertainty* as described above, associated with the fact that data is only available on a spatial grid.

(2) *Model uncertainty*, related to the fact that usually some model is used in converting observations into Eulerian velocity data. For example, sea-surface heights sensed by satellite are usually used as a scaled streamfunction for the velocity field, in view of the geostrophic assumption, which is of course only approximately correct.

(3) There is often *missing data*, for example in satellite sensing when clouds are present.

(4) *Nonuniformity* in the uncertainty is common, for example when using satellite data whose certainty diminishes further away from satellite tracks.

One way to think of dealing with these issues is to supplement the deterministic terms (for which one uses available data) with stochastic ones. In other words, the model for predicting the Lagrangian location of fluid parcels changes from an ordinary differential equation to a stochastic differential equation. This is a typical way to think of adding model uncertainty to any deterministic model which describes the evolution of a collection of state variables; in this example, the state variables represent the location, and the model consists of the unsteady Eulerian velocities which push the fluid parcels.

Recently, a method for characterizing the uncertainty in the time-evolving positions of fluid parcels was developed for two-dimensional flows for which Eulerian velocity data is available on a grid. The "stochastic sensitivity" field quantifies the eventual location uncertainty for each initial location of a fluid parcel, and is defined as the variance in the deviation from the trajectory from its deterministic prediction [1]. Non-uniform uncertainties in the model, e.g., when the tracks of satellites sensing ocean data only cover some areas, or when cloud cover impedes the gathering of data, can be incorporated into this model. However, the explicitly computable expressions for the stochastic sensitivity field could only be expressed in two dimensions.

This talk extends the concept of stochastic sensitivity to any general dimension, and moreover provides not just one number (the stochastic sensitivity) for each initial position, but rather gives an explicit expression for the uncertainty's spatial distribution in the limit of small uncertainty. The theoretical development requires understanding the difference of solutions of a stochastic differential equation with small noise in comparison with its deterministic counterpart. An intuitive method for this analysis would be to formally linearize the stochastic differential equation around the deterministic solution, and discard higher-order terms [5]. Doing so leads to a linearized differential equation for the stochastic component [5, 4]. If the noise in the original model were non-multiplicative - that is, it did not depend on the state of the evolving variable - then a closeness of the solutions to the stochastic and deterministic equations can be established in terms of the Kullback–Leibler divergence [4], thereby providing a possible justification for the linearization process. Other justifications appear in different contexts [3].

Permitting multiplicative noise is crucial in the geophysical applications, where the uncertainty is spatially dependent. Moreover, there is interest not just in establishing closeness of stochastic and deterministic solutions, but in obtaining

a computable uncertainty quantification or eventual Lagrangian trajectory locations. In this talk, it is shown that the distribution limits to a multivariate normal distribution (a Gaussian) with a (in general) non-diagonal covariance matrix, for any finite time. The covariance matrix can be explicitly computed using purely deterministic trajectories and the stochastic model for the data uncertainty, without having to perform expensive stochastic simulations. Two alternatives are presented for the covariance: an explicit analytical expression using the flow map of the deterministic flow, and a differential equation it obeys which can be used to provide a more efficient computation given Eulerian velocity data. The variance in the direction of greatest covariance is the stochastic sensitivity, which can be equivalently computed as the leading eigenvalue of the covariance matrix. The computability of this theoretical uncertainty distribution is demonstrated using oceanic velocity data. How to computationally leverage the obtained theory of multivariate normal distributions to numerically determine more general probability distributions in realistic settings is shown using the idea of Gaussian mixture models.

In summary, in assessing the transport of fluid parcels based on available unsteady Eulerian velocity data which is subject to spatial uncertainties, these tools provide a methodology for quantifying the impact of subgrid processes directly as a spatial probability distribution which evolves temporally.

References

[1] S. Balasuriya, *Stochastic sensitivity: A computable Lagrangian uncertainty measure for unsteady flows*, SIAM Review **62** (2020), 781–816–120.

[2] J. Berner et al, *Stochastic parameterization: Towards a new view of weather and climate models*, Bulletin of the American Meteorological Society **98** (2017), 565–588.

[3] Yu. Blagoveshchenskii, *Diffusion processes depending on a small parameter*, Theory of Probability and its Applications **VII** (1962), 130–146.

[4] D. Sans-Alonzo and A. Stuart, *Gaussian approximations of small noise diffusions in Kullback–Leibler divergence*, Communications in Mathematical Sciences **15** (2017), 2087–2097.

[5] S. Särkkä and A. Solin, *Applied Stochastic Differential Equations* (2019), Cambridge University Press.

Nonlinear dynamics of golden tides

Francisco J. Beron-Vera

(joint work with F. Andrade-Cano, G.J. Goni, D. Karrasch, M.J. Olascoaga and J. Triñanes)

Geometric fluid *mechanics* casts new light on the problem of *Sargassum* inundation, commonly referred to as golden tides, in the Caribbean Sea [2]. Pelagic *Sargassum* is a genus of large brown seaweed (a type of alga). A raft of pelagic *Sargassum* is composed of clumps formed by flexible stems which are kept afloat by means of bladders filled with gas. A raft drifts under the action of ocean currents and winds, subjected to physiological changes which are not considered here.

On one hand, recent nonlinear dynamical systems results pertaining to the fluid *kinematics* identify the carriers of *Sargassum* with coherent Lagrangian vortices whose (flow-invariant) boundaries defy stretching [5]. More specifically, such stretching defying boundaries are (closed) null-geodesics of the (indefinite) Lorenztian metric defined by the generalized Green–Lagrange strain tensor $E_\lambda(x) := C_t^{t+T}(x) - \lambda \mathrm{Id}$. Here $C_t^{t+T}(x)$ is the Cauchy–Green strain tensor, which objectively (i.e., in an observer-independent fashion) measures deformation over the finite time interval $[t, t+T]$ of material initialized at time t at each point x of two-dimensional domain. In turn, $\lambda > 0$ is a factor by which each subset of a closed null-geodesic of $E_\lambda(x)$ stretches (or shrinks) over $[t, t+T]$. When $\lambda = 1$ the arclength of the stretching defying boundary of a coherent Lagrangian vortex at time t is reassumed at time $t+T$. This property along with the area preservation property in the incompressible case conveys such boundaries extraordinary coherence. Moreover, it turns out that such λ-loops in general not only defy stretching but also resist diffusion [7]. And, numerically, they are observed to enclose [1] maxima of the deviation, with respect to the mean of the fluid mass, of the vorticity averaged along trajectories over $[t, t+T]$, denoted $\mathrm{LAVD}_t^{t+T}(x)$, [6].

The above generalized Kolmogorov–Arnold–Moser tori possess finite-time attractors for the cargo, viz., *Sargassum* rafts modeled as elastic networks of inertial (i.e., buoyant, finite-size) particles, which makes dragging by ocean currents and winds effective. More specifically, the networks are assumed to evolve according to a system of Maxey–Riley equations, modified for particles floating at the ocean–atmosphere interface, coupled by the linear-elastic spring forces acting between adjacent particles of the network [4]. Assume that the surface ocean velocity is in near geostrophic balance and the winds are sufficiently calm. Denote by x^* the location where the LAVD scalar field maximizes within a λ-loop at time t. By the smooth dependence of the solutions of the equations governing the motion of an elastic network of inertial particles, a network initially $O(\varepsilon)$-close to x^* will remain $O(\varepsilon)$-close to the trajectory flowing from it over a finite-time interval $[t, t+T]$. Denote by F_t^{t+T} the map that takes the particles forming the network at time t to their new positions at time $t+T$, and let k_{ij} be the stiffness of the spring connecting particle i with particle j. In [4] it is shown that $\det DF_t^{t+T} < 1$, that is, the *fluid* trajectory flowing from x^* is overall attracting over $[t, t+T]$, for all k_{ij} if the fluid mass enclosed by a coherent Lagrangian vortex (limited by a λ-loop) rotates anticyclonically, while if k_{ij} is sufficiently large when it does it cyclonically. It turns out that the condition on k_{ij} is easy to be satisfied, particularly when the number of particles forming a network is large, which typically is the case. One thus can expect that mesoscale ocean eddies in general represent traps for *Sargassum* rafts, which is consistent with evidence inferred from satellite images of the ocean surface.

On the other hand, a two-dimensional model of baroclinic Caribbean Sea eddy *dynamics*, with buoyancy inhomogeneity (e.g, [3]) and Lie–Poisson Hamiltonian structure, identifies thermal instability induced by bottom topography variation as a mechanism for filamentation and ensuing coastal inundation. More

specifically, the model equations can be cast in the form $\partial_t \mu = \{\mu, h\}$ for $\mu :=$ (q, ψ, q_2) where q_1 is the quasigeostrophic potential vorticity in the top of a system of two layers while q_2 is that in the bottom layer. The variable ψ is proportional to the buoyancy deviation from the reference buoyancy in the top layer, representing the (constant) reduced gravity g' corresponding to a nearby system with homogeneous fluid layers. The Hamiltonian is given by the system's energy, viz., $h[\mu] := \frac{1}{2} \int_D H_1 |\nabla \psi_1|^2 + H_2 |\nabla \psi_2|^2 + \frac{f_0^2}{g'} (\psi_1 - \psi_2)^2 \, d^2 x$. Here, ψ_1 and ψ_2 are the flow streamfunctions in the top and bottom layer, respectively, $H_1 = H$ and $H_2 = rH$, are the thicknesses of the layers at rest, and f_0 is the reference Coriolis parameter in the flow domain D. The bracket is given by $\{f, h\}[\mu] := \int_D \frac{q_1}{rH} \left[\frac{\delta f}{\delta q_1}, \frac{\delta h}{\delta q_1} \right] + \frac{\psi}{rH} \left(\left[\frac{\delta f}{\delta q_1}, \frac{\delta h}{\delta \psi} \right] - \left[\frac{\delta h}{\delta q_1}, \frac{\delta f}{\delta \psi} \right] \right) + \frac{q_2}{H} \left[\frac{\delta f}{\delta q_2}, \frac{\delta h}{\delta q_2} \right] d^2 x$. Here, the square bracket is the canonical Poisson bracket in $\mathbb{R}^2$. Let $\mathfrak{sdiff}(D)$ be the *Lie enveloping algebra* of $\text{SDiff}(D)$, the group of area preserving diffeomorphisms in D. The corresponding vector space is that of smooth time-dependent functions in D, denoted $\mathcal{F}(D)$, and the Lie bracket is given by $[\,,\,]$. The bracket $\{\,,\,\}$ is Lie–Poisson, representing a product for a *realization of a Lie enveloping algebra* on functionals in the dual (with respect to the L_2 inner product) of $\mathfrak{sdiff}(D) \times \mathfrak{sdiff}_s(D)$, where $\mathfrak{sdiff}_s(D)$ is the extension of $\mathfrak{sdiff}(D)$ by semidirect product to the vector space $\mathfrak{sdiff}(D) \times \mathcal{F}(D)$, with the representation of $\mathfrak{sdiff}(D)$ on $\mathcal{F}(D)$ given by $[\,,\,]$. When density inhomogeneity (temperature variation) is ignored in the upper layer, which makes $\{\,,\,\}$ a direct-product Lie–Poisson bracket, numerical simulations of the system initialized with a Gaussian vortex structure are seen to lead to the formation of a coherent Lagrangian vortex that propagates westward in a zonal channel with linearly decreasing depth to the west, minimally describing the bathymetry in the eastern Caribbean, with no noticeable distortion. But when temperature variation is allowed, the vortex filaments in a manner similar to typically shallow Caribbean eddies right before entering the western Caribbean. Such vortices are capable of attracting and carrying within *Sargassum* when they are coherent as discussed above. Thus thermal instability induced by bottom topography variation in the sense just described provides a mechanism for golden tides arrival on the coasts of the Yucatan Peninsula and Central America.

The results are consequential for the prediction of *Sargassum* arrival, and thus for response and planning.

REFERENCES

[1] F. Andrade-Canto, D. Karrasch, F.J. Beron-Vera, *Genesis, evolution, and apocalyse of Loop Current rings*, Phys. Fluids **32** (2020), 116603.

[2] F. Andrade-Canto, F.J. Beron-Vera, G.J. Goni, D. Karrasch, M.J. Olascoaga and J. Triñanes, *Carriers of* Sargassum *and mechanism for coastal inundation in the Caribbean Sea*, Phys. Fluids **34** (2022), 016602.

[3] F.J. Beron-Vera, *Extended shallow-water theories with thermodynamics and geometry*, Phys. Fluids **33** (2021), 106605.

[4] F.J. Beron-Vera, P. Miron, *A minimal Maxey–Riley model for the drift of* Sargassum, J. Fluid Mech. **904** (2020), A8.

[5] G. Haller, F.J. Beron-Vera, *Coherent Lagrangian vortices: The black holes of turbulence*, J. Fluid Mech. **731** (2013), R4.
[6] G. Haller, A. Hadjighasem, M. Farazmand, F. Huhn, *Defining coherent vortices objectively from the vorticity*, J. Fluid Mech. **795** (2016), 136–173.
[7] G. Haller, D. Karrasch, F. Kogelbauer, *Material barriers to diffusive and stochastic transport*, Proc. Nat. Acad. Sci. USA **115** (2018), 9074–9079.

Predicting spatiotemporal chaos by "learning" conjugate tubular neighborhoods

Nazmi Burak Budanur

Data-driven predictive models of spatiotemporally chaotic dynamics, see e.g. [1], are typically *black-box*, i.e. non-interpretable, systems and require large amounts of data to train. I argue that one can produce significantly simpler models if one aims to model the system not as whole but rather to generate an ensemble of models each of which applying to different subregions of the state space. For a demonstration, I consider the Kuramoto–Sivashinsky system arising from the discretization of the partial differential equation

$$(1) \qquad u_t + u_x u = -u_{xx} - u_{xxxx},$$

where the subscripts $_t$ and $_x$ denote partial derivatives with respect to time and space, respectively, and $u(x,t)$ is a scalar field satisfying the periodic boundary condition $u(x + L, t) = u(x, t)$. I fix the domain length as $L = 22.0$ and consider an $N = 30$-dimensional Fourier series discretization following Cvitanović et al. [2], who reported chaotic dynamics along with the unstable time-invariant solutions, e.g. (relative) equilbria and (relative) periodic orbits, in this system. My numerical experiments suggest that the chaotic trajectories of the system often visit the neighborhood of a *relative periodic orbit* which satisfy $u_p(x - \Delta x_p) = \Phi^{T_p}[u_p(x)]$, where Φ^t is the flow map implied by the numerical simulation of (1), $T_p \approx 32.80$ and $\Delta x_p \approx 10.96$. I propose to model the dynamics in the vicinity of this relative periodic orbit through a series of operations summarized as a block diagram in Fig. 1.
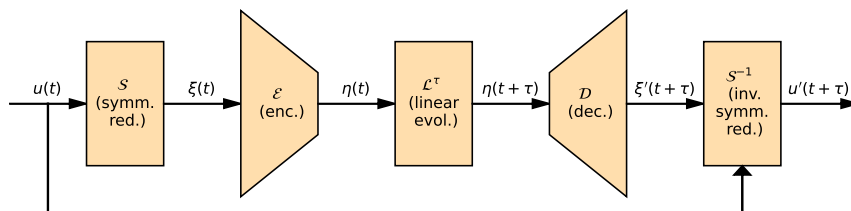

Figure 1. Block diagram depicting the series of operations for predicting the dynamics in the vicinity of a periodic orbit.

The first transformation shown in Fig. 1 is the symmetry reduction $\mathcal{S}$, which is a coordinate transformation that eliminates the symmetry degeneracy in the

data, without loosing any other dynamical information. In other words, $\xi = \mathcal{S}(u) = \mathcal{S}(\gamma u)$, where $\gamma \in \Gamma$ is a member of the symmetry group Γ such that an inverse $\mathcal{S}^{-1}(\xi) = \gamma' u$, where $\gamma' \in \Gamma$, can also be found. One can formulate such a transformation for the present system by combining the Fourier mode amplitudes such that the symmetry-reduced state variables' phases sum up to 2π under the action of symmetry operations as will be explained in [3].

The innermost block in Fig. 1 represents the linear time evolution $\eta(t+\tau) = \mathcal{L}^\tau \eta$ where $\eta \in \mathbb{R}^3$. The linear dynamics under $\mathcal{L}^\tau$ corresponds to the neighborhood of a periodic orbit which traces the unit circle in $\eta_1\eta_2$-plane with a period T_p and its Floquet multipliers are equal to the leading two Floquet multipliers of the original orbit. In the present case, these are a pair of complex multipliers $\Lambda_{1,2} = 0.3166 \pm i1.8136$ corresponding to an unstable manifold spiraling out of the orbit's tubular neighborhood. The assumption that underlie the model depicted in Fig. 1 is that the dynamics nearby the periodic orbit is dominated by its leading unstable subspace, thus, one can find a pair of encoder ($\mathcal{E}$) and decoder ($\mathcal{D}$) transformations that maps symmetry-reduced states ξ to the latent space η and back. I implement the transformations $\mathcal{E} : \mathbb{R}^N \to \mathbb{R}^3$ and $\mathcal{D} : \mathbb{R}^3 \to \mathbb{R}^N$ as multilayer perceptrons with two hidden layers of 128 nodes and sigmoid linear unit (SiLU) activation functions. I train these networks via stochastic gradient descent to minimize

$$(2) \quad \text{Loss} = \text{MSE}(\xi(t+\tau), \xi'(t+\tau)) + \text{MSE}(\mathcal{D}(\mathcal{E}(\xi(t))), \xi(t)) + \text{MSE}(\xi_p, \eta_p) \,,$$

where MSE is the "mean squared error", ξ are symmetry-reduced states in the periodic orbit's neighborhood, ξ' are the model predictions, ξ_p are the states on the periodic orbit, and η_p are those in the latent space. From left to right in (2) are the three error terms which I refer to as the prediction error, the auotencoder error, and the periodic orbit error terms. In my numerical experiments, I found the latter two to be necessary to prevent the networks from discovering an arbitrary mapping between the trajectories of two systems. I train the model by providing the algorithm with pairs of $(\xi(t), \xi(t+\tau))$, where $\tau \in [0, T_p)$, in randomly selected batches of 100 sampled from 1000 trajectories in the periodic orbit's neighborhood.

To test the model, I simulate a chaotic trajectory beginning from a random on-attractor initial condition and check the relative autoencoder error $\epsilon_{\text{AE}}(t) = \|\xi(t) - \mathcal{D}(\mathcal{E}(\xi(t)))\|/\|\xi(t)\|$ for the states along the trajectory. The left-most panels of Fig. 2 show two episodes (top and bottom) with initial conditions satisfying $\epsilon_{\text{AE}}(t) < 6\%$ projected onto the principal components of the periodic orbit in the symmetry-reduced state space (orange curves). The corresponding model predictions starting from the initial conditions are plotted green along with the periodic orbit in dashed blue. The projections labeled "latent space" show the same trajectories in the $\eta_1\eta_2$-plane, where the periodic orbit can be seen to be mapped onto the unit circle. Space-time visualizations show the chaotic trajectory segments next to their model predictions as color-coded amplitude of the scalar field $u(x, t)$. As shown, the simulated fields and their predicted counterparts are visually indistinguishable. My preliminary numerical experiments suggest that the episodes similar to those shown in Fig. 2 correspond to roughly a third of the total time evolution in
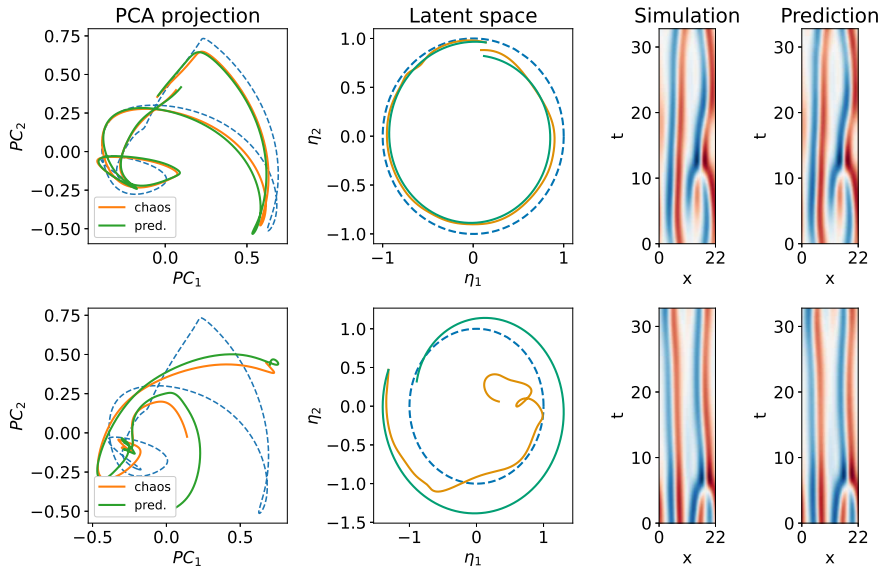
FIGURE 2. Two test episodes (top and bottom) sampled from a chaotic trajectory simulation and the corresponding model predictions visualized as projections from the symmetry-reduced space onto the principal components and in the latent space. Space-time plots visualize the amplitude of the scalar fields $u(x,t)$ of the simulated trajectories and the model predictions.

Kuramoto–Sivashinsky system at this domain size. I plan to report a detailed quantitative analysis and an additional model corresponding to the neighborhood of another periodic orbit in a future publication.

In summary, I demonstrated here that one could leverage the knowledge of periodic orbits to produce a predictive model of the Kuramoto–Sivashinsky system that captures a portion of the chaotic dynamics. I argue that in comparison to the black-box data-driven models, the present one offers a significant degree of interpretability since its latent-space dynamics is fully understood as a three-dimensional linear system.

REFERENCES

[1] J. Pathak, B. Hunt, M. Girvan, Z. Lu, and E. Ott, *Model-Free Prediction of Large Spatiotemporally Chaotic Systems from Data: A Reservoir Computing Approach*, Phys. Rev. Lett. **120** (2018), 024102

[2] P. Cvitanović, R. L. Davidchack, and E. Siminos. *On the state space geometry of the Kuramoto–Sivashinsky flow in a periodic domain.* J. Appl. Dyn. Syst. **9** (2010), 1–33

[3] S. Kneer, and N. B. Budanur, *Learning the dynamics of symmetry-reduced chaotic attractors from data (working title).* In preparation (2023).

Geostrophic Eddies Spread Near-Inertial Wave Energy to High Frequencies

OLIVER BÜHLER

(joint work with Wenjing Dong, K. Shafer Smith)

The generation of broadband wave energy frequency spectra from narrowband wave forcing in geophysical flows remains a conundrum. In contrast to the long-standing view that nonlinear wave-wave interactions drive the spreading of wave energy in frequency space, recent work suggests that Doppler-shifting by geostrophic flows may be the primary agent. We investigate this possibility by ray tracing a large number of inertia-gravity wave packets through three-dimensional, geostrophically turbulent flows generated either by a quasigeostrophic (QG) simulation or by synthetic random processes. We find that, in all cases investigated, a broadband quasi-stationary inertia-gravity wave frequency spectrum forms, irrespective of the initial frequencies and wave vectors of the packets. The frequency spectrum is well represented by a power law. A possible theoretical explanation relies on the analogy between the kinematic stretching of passive tracer gradients and the refraction of wave vectors. Consistent with this hypothesis, the spectrum of eigenvalues of the background flow velocity gradients predicts a frequency spectrum that is nearly identical to that found by integration of the ray tracing equations.

A 3D Lagrangian analysis of certain aspects of atmospheric circulation, with application to the 2019-2020 wildfire event

JEZABEL CURBELO

(joint work with Irina I. Rypina)

Throughout the 2019/2020 Australian bushfire season, wildfires gave rise to a concentrated plume characterized by an unprecedented amount of smoke within the lower stratosphere.

Motivated by this event, our study employs a dynamical system approach to investigate the three-dimensional atmospheric transport in the general region of the plume and identify key features of its temporal evolution. Specifically, aided by the Finite Time Lyapunov Exponent tool (FTLE), we identify Lagrangian Coherent Structures (LCS) that simplify the description of three-dimensional transport. The study is based on the atmospheric wind reanalysis model ERA5 [1] and involves the comparison of smoke plume simulations with available observations.

To begin, we compare the various formulations of FTLEs proposed in [2] to investigate the effects of vertical velocity and vertical shear on the movement of the plume. Stratospheric winds display relatively weaker vertical velocities compared to their horizontal counterparts. However, we show that the quasi-2D approach overlooks the fact that even minor vertical displacements can subject air parcels to distinct horizontal advection patterns driven by strong vertical shear. As a
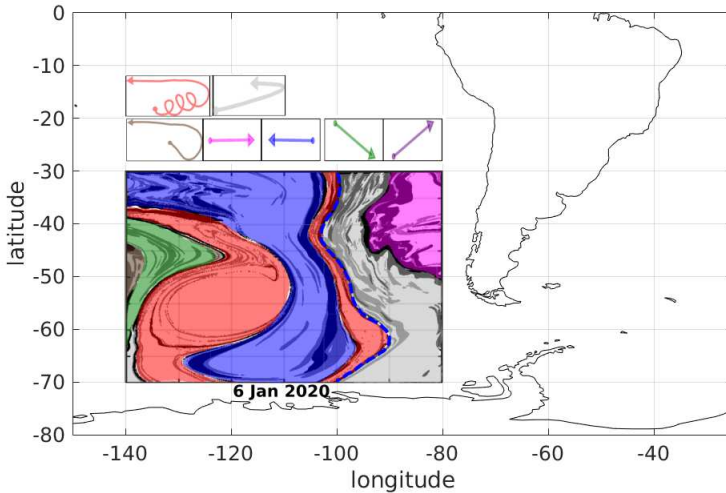
FIGURE 1. Simplified scheme of forward path types initialized on January 6, 2020, in different regions (indicated by colors) at an 18 km height, considering constant buoyancy. Specifically, a value of 0.0022 m/s is added to the vertical velocity. Forward FTLE is represented in black and gray for $\tau = 20$ and $\tau = 40$ days, respectively. The red trajectory corresponds to path P1, and the magenta one corresponds to path P2.

result, achieving an accurate representation of three-dimensional transport necessitates considering trajectory movements in all three dimensions and, significantly, incorporating the vertical shear terms into the formulation of the FTLE matrix.

Some of the uncovered Lagrangian Coherent Structures (LCS) that are directly relevant to the evolution of the smoke plume from the wildfire event of 2019-2020 are considered in detail. Additionally, other LCS that are less relevant to the plume but exhibit interesting geometries are examined, such as the presence of 3D lobe dynamics at play.

The movement of smoke plumes is significantly influenced by the buoyancy of hot smoke, as indicated by the analysis of simulated trajectories in the ERA reanalysis model. We estimated the time-averaged buoyant velocity by comparing the altitude difference between the simulated and observed P1 trajectories on February 26th. Incorporating this buoyant velocity into the ERA5 velocities led to a substantial improvement in agreement with observations.

Figure 1 illustrates the distribution of LCS on January 6th, coinciding with the detection of a highly organized smoke patch observed from satellites nearly halfway across the globe from Australia. This coherent patch bifurcated into two segments: one tracing a westward trajectory towards Australia at significantly higher altitudes (P1), and the other progressing eastward at lower altitudes (P2). The partitioning of the plume into P1 and P2 on January 6th strongly indicated the presence of robust LCS in the area at that specific time. These LCS acted as effective transport barriers, dictating distinct trajectory outcomes for parcels situated on opposing sides of the LCS.

In fact, the FTLE map depicted in Figure 1 displayed numerous prominent ridges, serving as proxy LCS. These ridges outlined distinct zones within the region, each characterized by qualitatively distinct behaviors of fluid parcels. The schematic representations of trajectories initialized in various regions are also presented in Figure 1. Particularly noteworthy are the regions colored in red and magenta, corresponding to the paths followed by P1 and P2, respectively, which are of primary interest to our study.

The former originates from an eddy-like feature centered around 125W, 55N, characterized by two elongated and slender tendrils extending from its core. On the other hand, the latter originates in the eastern section of the domain and is isolated from the surrounding regions by a robust FTLE ridge. This ridge exhibits a three-dimensional tilted-curtain-line geometry, spanning the altitudes of the observed plume (16-22 km), which is highlighted with a dashed blue line in the figure.

This eddy feature had a notable impact on the evolution of the smoke plume [3, 4]. We investigate its formation, which took place around the same time and in close proximity to the area of intense wildfires. Furthermore, we analyze its subsequent evolution. For example, during the entrainment of the smoke plume, we observed the formation of a dipole structure, wherein the smoke was concentrated solely within the anticyclonic portion. Finally, we describe how this structure sustained its coherence over an extended period. Further details can be found at [5].

References

[1] H. Hersbach, B. Bell, P. Berrisford, A. J. M. S. Horányi, J. Muñoz Sabater, J. Nicolas, R. Radu, D. Schepers, A. Simmons, C. Soci, et al. Global reanalysis: goodbye ERA-interim, hello ERA5. *ECMWF newsletter*, 159:17–24, 2019.

[2] Mohamed H. M. Sulman, Helga S. Huntley, B. L. Lipphardt, and A. D. Kirwan. Leaving flatland: Diagnostics for lagrangian coherent structures in three-dimensional flows. *Physica D: Nonlinear Phenomena*, 258:77–92, 2013.

[3] S. M. Khaykin, B. Legras, S. Bucci, P. Sellitto, L. Isaksen, F. Tence, S. Bekki, A. Bourassa, L. Rieger, D. Zawada, et al. The 2019/20 Australian wildfires generated a persistent smoke-charged vortex rising up to 35 km altitude. *Communications Earth & Environment*, 1(1):1–12, 2020.

[4] G. P. Kablick, D. R. Allen, M. D. Fromm, and G. E. Nedoluha. Australian Pyrocb Smoke generates synoptic-scale stratospheric anticyclones. *Geophysical Research Letters*, 47(13):e2020GL088101, 2020.

[5] J. Curbelo, I. I. Rypina. A three dimensional Lagrangian analysis of the smoke plume from the 2019/2020 Australian wildfire event. (Available at `https://doi.org/10.1002/essoar.10512436.1`, Submitted 2023.).

Drifter-Based Analysis of a Coherent Submesoscale Eddy in the Balearic Sea

MICHAEL DOTZEL

(joint work with Irina I. Rypina, Larry Pratt)

On March 1st 2022, a suite of drifters resolving flow speeds at different depths were deployed at the northeast periphery of a particularly coherent eddy of radius approximately 4 km. This suite was comprised of 9 CARTHE and 3 CODE drifters (surface), 10 SVP drifters (15 m), and 9 each of WHOI "holey sock" drifters capturing speeds at 8, 22, 35, and 50 m depths, the bulk of which survived for 2 weeks before dying. A linear least squares approach to calculating horizontal velocity gradients for drifters at each depth reveals subsurface depth-uniformity in vorticity (around 2f) and surface signatures of around 3f, with divergence around 0.5f (peaking at ± f) at all depths. Tilting, stretching, and additional terms in the vorticity balance are all of the same order of magnitude, indicating no particular dynamic responsible for maintaining the eddy. The velocity field obtained by applying drifter data to a Gaussian Process Regression reveals that for two weeks, the eddy does not appreciably change in size (radius remains at about 4 km at all subsurface depths) but the velocity gradually decays in both depth and time. Due to the lack of observations available outside of the eddy, however, Lagrangian estimates such as LAVD and FTLE are somewhat unreliable in demonstrating the observed coherence of the eddy.

REFERENCES

[1] Molinari, R., and A. D. Kirwan, 1975: Calculations of Differential Kinematic Properties from Lagrangian Observations in the Western Caribbean Sea. J. Phys. Oceanogr., 5, 483–491.

[2] Rypina, I. I., T. R. Getscher, L. J. Pratt, and B. Mourre, 2021: Observing and Quantifying Ocean Flow Properties Using Drifters with Drogues at Different Depths. J. Phys. Oceanogr., 51, 2463–2482.

[3] Haller, G., Hadjighasem, A., Farazmand, M., and Huhn, F. (2016). Defining coherent vortices objectively from the vorticity. Journal of Fluid Mechanics, 795, 136-173. doi:10.1017/jfm.2016.151.

Coherence timescales, fronts, and dynamic regime change (a sketch)
GARY FROYLAND
(joint work with Michael C. Denes, Shane R. Keating, Péter Koltai)

Our goal was to illustrate how dynamic operator-theoretic techniques can be help to analyse and understand geophysical phenomena. We began by recapping the definition of the *dynamic Laplacian* [1], which defines a dynamic spectral geometry for dynamical systems. The leading nontrivial eigenvalue of the dynamic Laplacian quantifies the exponential global mixing that occurs on the geophysical domain over the time duration of computation. The corresponding eigenfunction reveals the dominant coherent sets in the domain.

Sometimes there is clear time duration over which Lagrangian computations should be made, but often the choice of flow time is a matter of trial and error. In the first part of the talk, we introduced the notion of *maximal coherence timescale* as the time duration over which the mixing rate per unit time is minimized; equivalently the duration over which coherence is maximized. We illustrated the computation of this timescale for a single ocean eddy and a field of ocean eddies. The maximal coherence timescale is the shortest of three timescales we discussed. A longer timescale is the *median residence time* of an ocean eddy, where we have identified the ocean eddy using an eigenfunction of the dynamic Laplacian, computed over the maximal coherence timescale. The median residence time is the time that it takes for half of the water in the eddy to be flushed out, and is of clear importance for quantifying eddy transport. The third and longest timescale is the *tracking time*; the time over which an Eulerian or Lagrangian method can discern a continuous signature of an eddy. This latter time is often provided as the "eddy lifetime" in the literature, even though the eddy may be completely flushed, perhaps more than once. Therefore tracking time is less relevant for seawater transport. In our experiment we found a maximal coherence timescale of 38 days, a median residence time of 140 days, and a tracking time in excess of 250 days. These definitions are crucial for careful definitions of transport (such as ocean eddies) and we recommend their use in transport calculations.

The dynamic Laplacian was then applied to identify Southern Ocean fronts directly from water parcel trajectories, without any inference from physical water properties such as temperature, salinity, etc... Fronts were defined as level-set contours of the leading dynamic Laplacian eigenfunction, where the dynamic Laplacian was computed over 540 days, the mean circumnavigation time for water parcels around Antarctica. We found that these dynamically defined fronts often coincided with sharp gradients in physical scalar fields such as sea-surface height and temperature, and to a lesser extent, salinity, even though these scalar fields were instantaneous snapshots, rather than having a 540-day Lagrangian history. By comparing fronts with pullbacks of 30-day ahead fronts, we can quantify and map northward and southward flux out of/into daily sequences of fronts. Averaging such daily 30-day fluxes over 4.5 years we obtain a composite picture of north/south cross-frontal transport [3]. This novel cross-frontal transport map

is highly structured and unlike similar maps in the literature. We believe that sea floor bathymetry may play a key role in the transition from northward to southward transport and vice-versa.

Finally, to tackle the problem of automatic identification of birth and death of coherent features, we introduced an *inflated dynamic Laplacian* on a time-expanded domain. On each time fibre, we endow the domain with a pullback metric (pulling back the Euclidean metric from the future time). The distinct time fibres are connected by a one-dimensional diffusion across the single time dimension. A substantial theory connecting dynamic geometry with the spectrum of the inflated dynamic Laplacian is contained in [4]. We used the leading two eigenfunctions of the inflated dynamic Laplacian to capture a Southern polar vortex breakup event. The timing and spatial extent of the loss of coherence during the breakup is clearly distinguished by the eigenfunctions.

REFERENCES

[1] Gary Froyland. *Dynamic isoperimetry and the geometry of Lagrangian coherent structures.* Nonlinearity, 28:3587-3622, 2015
[2] Michael C. Denes, Gary Froyland, and Shane R. Keating. *Persistence and material coherence of an ocean eddy.* Physical Review Fluids, 7(3):034501, 2022.
[3] Michael Denes, Shane R. Keating, and Gary Froyland. *Bathymetry imposes a global pattern of cross-front transport in the Southern Ocean.* arXiv, 2023.
[4] Gary Froyland and Péter Koltai. *Detecting the birth and death of finite-time coherent sets.* Communications on Pure and Applied Mathematics. 2023

Subgridscale parametrization via machine learning from noisy observations: deterministic and stochastic approaches

GEORG GOTTWALD

(joint work with Sebastian Reich)

We consider the closure problem of subgridscale parametrization in multiscale systems. Given a slow=fast system the aim is to find a reduced effective equation for the slow dynamics only. We present two separate methods to determine the closure term from noisy observations: a deterministic approach and a stochastic approach.

The deterministic approach employs a simple random feature maps machine learning architecture the parameters of which are learned sequentially using data assimilation. The data assimilation component controls the observational noise. To account for eventual stochasticity of the closure term we introduce a Langevin sampler based on diffusion maps to draw samples from the distribution of the closure term.

Identifying Missing Dynamics with Machine Learning Algorithms
John Harlim

In the talk, I will discuss a general closure framework to compensate for the model error arising from missing dynamical systems. The proposed framework reformulates the model error problem into a supervised learning task to estimate a very high-dimensional closure model, deduced from the Mori-Zwanzig representation of a projected dynamical system with a projection operator chosen based on Takens embedding theory [3, 1, 2]. Besides theoretical convergence, this connection provides a systematic framework for closure modeling using available machine learning algorithms. I will demonstrate supporting numerical examples in predicting spatiotemporal chaotic systems, including the 57-mode barotropic stress models with multiscale interactions that mimic the blocked and unblocked patterns observed in the atmosphere and the Kuramoto-Sivashinsky equation which spatiotemporal chaotic pattern formation models trapped ion mode in plasma and phase dynamics in reaction-diffusion systems [2].

The second part of this talk concerns the applications of the proposed closure framework to statistical closure problems [4, 5]. One of the difficulties in this statistical closure problem is the lack of training data, which is a configuration that is not desirable in supervised learning with neural network models. In this study with the 40-dimensional Lorenz-96 model, the shortage of data is due to the stationarity of the statistics beyond the decorrelation time. Thus, the only informative content in the training data is from the short-time transient statistics. Beyond the training data issues, the closure problem has several practical challenges in non-homogeneous statistical regimes. That is, we need to ensure that the closure model produces positive-definite covariance matrix estimation yet overcomes the inherent instability of the stochastic fluctuation dynamics.

The final topic of the talk is on deducing error bounds and mathematical conditions that allow for the estimated model (attained by machine learning algorithm) to reproduce the underlying stationary statistics, such as one-point statistical moments and auto-correlation functions, in learning Ito diffusions [6]. Based on the perturbation theory of ergodic Markov chains and the linear response theory, we deduce a linear dependence of the errors of one-point and two-point invariant statistics on the error in the learning of the drift and diffusion coefficients. We examine the mathematical conditions for the theoretical error bounds on two well-understood learning algorithms: the kernel-based spectral regression method and the shallow random neural networks with the ReLU activation function.

References

[1] Faheem Gilani, Dimitrios Giannakis, and John Harlim. *Kernel-based prediction of non-markovian time series.* Physica D: Nonlinear Phenomena, **418** (2021) 132829.

[2] John Harlim, Shixiao W Jiang, Senwei Liang, and Haizhao Yang. *Machine learning for prediction with missing dynamics.* Journal of Computational Physics, **428** (2021)109922.

[3] Shixiao W Jiang and John Harlim. *Modeling of missing dynamical systems: Deriving parametric models using a nonparametric framework.* Research in the Mathematical Sciences, 7 (2020)1–25.

[4] Di Qi and John Harlim. *Machine learning-based statistical closure models for turbulent dynamical systems.* Philosophical Transactions of the Royal Society A, **3**80 (2022) 20210205.

[5] Di Qi and John Harlim. *A data-driven statistical-stochastic surrogate modeling strategy for complex nonlinear non-stationary dynamics.* Journal of Computational Physics, **485** (2023) 112085.

[6] He Zhang, John Harlim, and Xiantao Li. *Error bounds of the invariant statistics in machine learning of ergodic Itô diffusions.* Physica D, **427** (2021)133022.

SWOT: A wonderful new era of upper ocean physics
Darryl Holm
(joint work with Albert Dombret, Ruiao Hu and Oliver D. Street)

Can waves amplify currents? We discuss a new wonderful theory of deterministic and stochastic transport in upper ocean dynamics (STUOD).

The ocean surface is a compound dynamical system of waves forced by the wind and propagating on fluid currents. The wind's force induces a rate-of-change of horizontal wave momentum, which couples to the fluid current via the Kelvin circulation theorem for the sum of the wave momentum plus the current momentum.[1]

The fluid current *transports* mass, while the waves *propagate* phase $\phi(x, t)$ in the moving frame of the current flow. The dynamics for this compound system can be derived from Hamilton's principle, $\delta S = 0$ for $S = \int L \, dt$, written for reduction by symmetry [6] of the sum of three Lagrangians

$$
\begin{aligned}
L &= L_{fluid}(g_t, \dot{g}_t, a_0) + L_{wave}(\dot{\phi}, d\phi) + L_{int} \\
&= L_{fluid}(\dot{g}_t g_t^{-1}, a_0 g_t^{-1}) + L_{wave}(\dot{\phi} g_t^{-1}, d\phi g_t^{-1}) + L_{int} \\
&= \ell_{fluid}(\mathbf{u}, a_t) + \ell_{wave}(\dot{\phi} g_t^{-1}, d\phi g_t^{-1}) + \ell_{int}(N\mathbf{u} \cdot \nabla \phi)
\end{aligned}
$$

The quantity a_0 represents initial conditions of passively advected variables (tracers) such as mass density, evolving as $a_t = a_0 g_t^{-1}$ by the push-forward action of the time-dependent flow map g_t.

The reduced interaction Lagrangian ℓ_{int} is a functional of both wave and fluid variables. The coupling in the reduced Lagrangian ℓ_{int} for wave, mean flow interaction (WMFI) is the momentum map for the wave degree of freedom that is carried by the fluid. In ℓ_{int}, this momentum map is paired in the L^2 sense with the velocity of the fluid current. This pairing takes the wave dynamics into the frame of motion of the fluid. Upon taking the variation of $\ell_{fluid} + \ell_{int}$ in the fixed Eulerian frame wrt the fluid velocity, $\mathbf{u}$, one obtains the total wave + fluid momentum.

---

[1]Wave breaking impulses also transfer horizontal wave momentum to fluid momentum. However, wave breaking is far more local, random, dissipative, and uncertain than the shift of wave momentum by wind forcing followed by the fluid circulation induced from the Kelvin theorem by the non-inertial force of frame change from the Eulerian frame into the fluid frame. Wave breaking impulses would be represented variationally by using the Lagrange-d'Alembert method to introduce space-time stochastic forcing in the fluid motion equation in the Eulerian frame.

In the corresponding Hamiltonian formulation of WMFI, the total wave + fluid momentum appears in the upper left corner of the upper-left block diagonal semidirect-product Lie-Poisson operator. That is, the upper-left block diagonal is a Lie-Poisson bracket. In this upper left corner of the Lie-Poisson operator, the vector field for the fluid velocity, $\mathbf{u}$, Lie transports the total wave + fluid momentum as well as the advected fluid variables, a_t, with the Lie-derivative action of the fluid velocity vector field.

In the integrand of the corresponding Kelvin circulation theorem, the Eulerian fluid circulation velocity is measured relative to the wave momentum per unit mass, which is proportional to the local group velocity of the wave degree of freedom. The wave momentum per unit mass then plays the role of the Stokes drift velocity in the Craik-Leibovich 'vortex force' in the creation of Langmuir circulations. This observation was augmented by explaining how the deterministic WMFI equations could be made stochastic by modifying the loop integral in the the WMFI Kelvin-Noether theorem to make its velocity stochastic in the sense of Stratonovich [2, 3, 4, 5].

The lower-right block-diagonal of this (untangled) Poisson operator acts on variations of the Hamiltonian with respect to the wave variables; namely, the wave action density $N\,d^2x$ and the wave vector $\mathbf{k} := \nabla\phi$. The lower-right block of the block-diagonal Poisson operator can be either a symplectic 2-cocycle (when the order parameter is a scalar), or it can be a generalised 2-cocycle with L^2-dual covariant derivatives (when the wave order-parameter dof that transforms according to the Lie algebra of the remaining part of the broken symmetry is non-Abelian). The non-Abelian case occurs in condensed matter theories of liquid crystals and spin glasses, for example.

For waves on the ocean surface and for internal waves in the ocean, the reduced interaction Lagrangian $\ell_{int} = \int \mathbf{u} \cdot N\nabla\phi\,d^2x$ is the product of the wave action density ($N\,d^2x = \delta L_{wave}/\delta\dot{\phi}$) times the Doppler shift of the wave frequency ($\mathbf{u}\cdot\mathbf{k} = \mathbf{u} \cdot \nabla\phi, u = \dot{g}_t g^{-1}$) that arises from the shift of the Lagrangian for the wave phase dynamics into the moving frame of the fluid current.

Mathematically, from our earlier work on the dynamics of complex fluids such as liquid crystals [1], we know this representation of ocean surface dynamics follows from Lagrangian reduction by stages for the push-forward of the composition of diffeomorphisms (or diffeos: smooth invertible maps of the reference configuration of the fluid into its present configuration in the flow domain) acting on functionals of space-time derivatives of phase ($\dot{\phi}, d\phi$), first by right action of 1D unitary transformations to obtain wave phase dynamics, then by right action of diffeos on the tangent space of the fluid flow map ($g_t, \dot{g}_t$) and on the phase-reduced wave variables to shift them both into the Eulerian fluid representation.

Motivated by the recent first-look satellite image data from the NASA and ESA SWOT (Surface Water and Ocean Topography) mission [7], the talk and its slides illustrated the approach described above for compound wave-current interaction in the cases of the Burgers-KdV current-wave configuration dynamics in both 1D

and 2D. The 1D Burgers-KdV case showed a variety of interesting nonlinear wave-current interactions. The 2D case was actually Euler-KdV rather than Burgers-KdV. Since no simulations had yet been accomplished for the latter 2D case the question arose whether the interesting compound soliton traveling wave solutions in the 1D Burgers-KdV case would persist in the 2D Euler-KdV case. This issue arising from discussions will be addressed in future work.

REFERENCES

[1] Holm, D. D., 2002. Euler-Poincaré dynamics of perfect complex fluids. *Geometry, Mechanics, and Dynamics*, 169-180. Retrievable from `https://doi.org/10.1007/0-387-21791-6_4`
[2] Holm, D.D., 2015. Variational principles for stochastic fluid dynamics. Proceedings of the Royal Society A: Mathematical, Physical and Engineering Sciences, 471(2176), p.20140963. Retrievable from `https://doi.org/10.1098/rspa.2014.0963`
[3] Holm, D. D. (2019). Stochastic closures for wave-current interaction dynamics. Journal of Nonlinear Science, 29 , 2987-3031. Retrievable from `https://doi.org/10.1007/s00332-019-09565-0`
[4] Holm, D. D., Hu, R., & Street, O. D. (2022a). Coupling of waves to sea surface currents via horizontal density gradients. Retrievable from `http://arxiv.org/abs/2202.04446`
[5] Holm, D. D., Hu, R., & Street, O. D. (2022b). Lagrangian reduction and wave mean flow interaction. Retrievable from `http://arxiv.org/abs/2301.04121`
[6] Holm, D.D., Marsden, J.E. and Ratiu, T.S., 1998. The Euler-Poincaré equations and semidirect products with applications to continuum theories. Advances in Mathematics, 137(1), pp.1-81. Retrievable from `https://doi.org/10.1006/aima.1998.1721`
[7] NASA-SWOT Surface Water and Ocean Topography, 2023. `https://swot.jpl.nasa.gov`

Global strong solutions for the 3D primitive equations with negative viscosity kinetic energy backscatter parametrization

PAUL HOLST

The energy of turbulent flows transfers between large and small scales. Since numerical simulations of ocean models require discretizations of the equations of motion, there is a finite cutoff scale beyond which motion is not resolved. One idea to reduce the associated overdissipation of energy is a numerically motivated backscatter parameterization, where the term energy backscatter is, in physical terms, a term for a missing energy transfer from the unresolved scales to the resolved flow. Here, we are interested in results about the well-posedness of ocean models provided with such backscatter parametrizations. In this project, the inital-boundary value problem of the continuous 3-dimensional primitive equations of the ocean with a negative kinetic energy backscatter parametrization is studied. More precisely, the existence and uniqueness of a global strong solution are established.

Co-recurrent SST-SAT States Indicate Strong-impact Events over Tropical Pacific

Yu Huang

(joint work with Ming Shi, Zuntao Fu)

Sea surface temperature anomalies (SSTA) over the tropical Pacific, including events like El Niño-Southern Oscillation (ENSO), can lead to intensified air-sea interactions and various climate impacts. As a result, monitoring regional SSTA and its interaction with the atmosphere is of significant importance. While several indices based on area-mean SSTA are used to describe the magnitude of these events, the area-mean processing often overlooks valuable dynamical information due to the cancellation of local negative and positive anomalies.

By embedding spatio-temporal data into the state space, it becomes possible to measure the local dynamical states of the underlying system along its temporal evolution. This approach provides an alternative to the traditional area-mean processing. Faranda et al. [4] introduced the Dynamical Systems Metric (DSM), which measures the instantaneous values of persistence and dimension for a given system. Additionally, DSM allows for the estimation of the co-recurrence ratio between two systems, such as SSTA and the overlaying surface air temperature anomalies (SATA).

Compared to covariance analysis, which considers the entire probability distribution of variables, DSM focuses more on the tail of the probability distribution. This characteristic makes DSM particularly useful for analyzing extreme events. Therefore, applying DSM offers a new and promising way to monitor SSTA and the atmosphere over the tropical Pacific region. It provides valuable insights into the local dynamics and interaction patterns of the underlying systems, enabling a more comprehensive understanding of climate phenomena and their broader climate impacts.

In this report, I present a systematic investigation focusing on the co-recurrence ratio between SSTA and their overlaying atmospheric fields over the tropical Pacific. The analysis of high co-recurrence ratios reveals events characterized by strong air-sea interactions and feedback, leading to significant weather impacts not only around the Pacific but also in remote regions.

One of the notable findings of this study is the explanation of the relatively weak impact of the super El Niño in 2015/2016. The air-sea co-recurrence ratio sheds light on the ENSO diversity and asymmetry, providing valuable insights into the underlying mechanisms of these phenomena. Moreover, the index introduced in this report proves to be effective in identifying unusual neutral days with prolonged strong air-sea couplings. Unlike regular ENSO events, these days exhibit less homogeneous SST anomaly distributions, yet they have caused intense climate impacts. Understanding and monitoring such occurrences can be crucial for predicting and managing climate-related impacts in various regions.

The investigation also emphasizes the examination of various magnitude levels of SST-SAT co-recurrence ratio and its corresponding impacts on the atmosphere.

Specifically, the results demonstrate that the instantaneous persistence and dimension of SATA have strong connections with the co-recurrence ratio, particularly for extreme values, and they display the ability to distinguish between different types of El Niño events. Furthermore, the study delves into the climate impacts arising from distinct El Niño events and reveals that these impacts can be differentiated based on the SST-SAT co-recurrence ratio. Notably, the study identifies that the divergent effects on global climate teleconnections are primarily present in the upper troposphere.

Overall, this systematic investigation on the co-recurrence ratio between SSTA and its overlaying atmospheric fields offers a new perspective on analyze the air-sea interactions in the tropical Pacific. It also shows the promising ability of DSM applied to air-sea interactions in climate studies, allowing for extracting more valid dynamical information of climate events from the spatio-temporal dataset.

Whereas there still exist open questions for analyzing the air-sea co-recurrence. One is whether the instantaneous persistence, dimension and co-recurrence ratio can be used as prediction factors to forecast the climate impacts, which has not been explored. Second is that the co-recurrence ratio by DSM cannot infer causal direction from the air-sea interactions, which needs further technical efforts. Third is that the long-term variability of the SSTA is with considerable uncertainty, and it is still unknown whether DSM can infer long-term variations from the SSTA data.

References

[1] Y. Huang, N. Yuan, M. Shi, et al., *On the Air-Sea Couplings Over Tropical Pacific: An Instantaneous Coupling Index Using Dynamical Systems Metrics*, Geophysical Research Letters **49** (2022), e2021GL09704.
[2] Y. Huang, M. Shi, Z. Fu, *A Dynamical Systems Perspective to Characterize the El Niño Diversity in Spatiotemporal Patterns*, Frontiers in Physics **10** (2022), 919951.
[3] M. Shi, Y. Huang, Z. Fu, *Dynamical systems persistence parameter of sea surface temperature and its associations with regional averaged index over the tropical Pacific*, International Journal of Climatology **42** (2022), 7550–7562.
[4] D. Faranda, G. Messori, P. Yiou, *Diagnosing concurrent drivers of weather extremes: application to warm and cold days in North America*, Climate Dynamics **54** (2020), 2187–2201.

The Lagrangian Dynamics of Kinematic Properties in the Ocean

Helga S. Huntley

(joint work with A. D. Kirwan, Jr., James Turbett)

A number of recent large drifter deployments have resulted in a wealth of data on trajectories in the ocean, which in turn are leading to new insights into the transport and dispersion properties and, by extension, into the velocities and velocity gradients of the underlying currents. The kinematic properties (KPs), i. e., normal and shear deformation rates (a and b, respectively), relative vorticity (c), and divergence (d), can be estimated from a group of drifters based either on a least squares (energy minimizing) fit to a linearization around the cluster

centroid position or velocity [3, 4], on the change in area of a convex hull of the drifter positions (and "area" in transformed coordinates) [3] or integration around the boundary of the convex hull [2], or on gradients computed on a statistically interpolated velocity field [1]. This framework naturally gives rise to Lagrangian KP time series.

These observations have motivated a new look at the KP evolution equations, first derived by Petterssen [5] and considered in the context of synoptic-scale atmospheric circulation. With the application to near-surface oceanic drifter observations in mind, the equations have here been modified to apply to motion at a fixed depth over time and space scales of the order of days and kilometers. The starting point are the two-dimensional equations of motion for the velocity components (u, v)

(1) $$\dot{u} - fv = \mathbf{F}^x,$$

(2) $$\dot{v} + fu = \mathbf{F}^y,$$

where f is the Coriolis parameter and the external forcing terms are kept generic, potentially representing baroclinic torque, wind stress curl, geopotential gradients, etc. They are summarized in terms of a velocity potential Φ and a stream function Ψ:

(3) $$\mathbf{F} = \langle \mathbf{F}^x, \mathbf{F}^y \rangle = \nabla \times [\mathbf{k}\Psi + \nabla \times (\mathbf{k}\Phi)]$$

A quadratic Taylor expansion of Ψ and Φ, differentiation, and simplification results in a set of non-linearly coupled ordinary differential equations describing the along-trajectory temporal evolution:

(4)
$$
\begin{aligned}
\dot{a} + da - fb &= 2(\hat{A} - \hat{C}) + 2B \\
\dot{b} + db + fa &= -2(A - C) + 2\hat{B} \\
\dot{c} + dc + fd &= -2(A + C) \\
\dot{d} + \frac{1}{2}(d^2 + f^2 + a^2 + b^2 - (c + f)^2) &= 2(\hat{A} + \hat{C}).
\end{aligned}
$$

Thus, the coupling occurs due to the divergence d appearing in all equations and all KPs appearing in the d-equation.

The solution space even for simple steady forcing turns out to be quite complex, sensitive to both forcing and initial conditions. Here, only a small subset of the 10-dimensional parameter space is explored by systematically varying initial conditions and forcing terms, further assuming that the latter remain constant.

Generally, for a given constant forcing, there are two steady-state solutions. In most (although not all) cases, these are characterized by positive and negative absolute vorticity ($\xi := c + f$), respectively. Their stability is a function of the particular choice of the forcing.

The homogeneous case (zero external forcing) exhibits a fundamental instability when $c = -f$, reminiscent of the classic Raleigh-Taylor inertial instability found in rotating fluids. Solutions are stable if and only if absolute vorticity dominates total deformation rate, i. e., $\xi^2 > a^2 + b^2$, indicating a central role for the generalized

Okubo number $G = a^2 + b^2 - \xi^2$, using the absolute vorticity. All stable solutions are inertially periodic or constant. Further, total deformation rate, absolute vorticity, and the combination $H = d^2 + f^2 - G = d^2 + f^2 - a^2 - b^2 + \xi^2$ are dynamically conserved, in the sense that their product with dilation $\delta = \exp(\int_0^t d(\tau)d\tau)$ (path-integrated divergence) is constant along trajectories.

Constant hyperbolic forcing of the form $A = C = \hat{A} = \hat{C} = 0$, $B \neq 0$ and/or $\hat{B} \neq 0$ permits as stable solutions only the two steady-states. All other initial conditions lead to instabilities with divergence tending to $-\infty$.

Constant elliptic forcing of the form $B = \hat{B} = 0$, $A = C$, and $\hat{A} = \hat{C}$ exhibits different behavior, which also depends on whether $A \neq 0$ and/or $\hat{A} \neq 0$. In particular, both stable and unstable solution arise. For pure Ψ-forcing ($A \neq 0$), stable solutions converge to the steady state with positive divergence. This is also the case if $\hat{A} > f^2/8$. Stable solutions for $\hat{A} < f^2/8$, on the other hand, are oscillatory, with periods that can be sub- or superinertial. Moreover, the period is the same for $a^2 + b^2$, c, and d, but is frequently different for the individual deformation rates a and b.

These complexities of the solution space arise, in spite of the deceptively simple setting. They illustrate that observed KP time series cannot be interpreted in isolation, as divergence, vorticity, and deformation rate are intimately linked. Moreover, observed periodicities in these time series do not necessarily reflect periodicities in the external forcing: Inertial oscillations arise intrinsically, and both sub- and superinertial oscillations can occur with constant forcing.

References

[1] R. C. Gonçalves, M. Iskandarani, T. Özgökmen, W. C. Thacker, *Reconstruction of Submesoscale Velocity Field from Surface Drifters*, J. Phys. Oceanogr. **49**, (2019) 941–958.
[2] H. Kawai, *Scale dependence of divergence and vorticity of near-surface flows in the sea. Part 1. Measurements and calculations of area-averaged divergence and vorticity*, J. Oceanogr. Soc. Jpn. **41** (1985) 157–166.
[3] R. Molinari, A. D. Kirwan Jr., *Calculations of differential kinematic properties from Lagrangian observations in the Western Caribbean Sea*, J. Phys. Oceanogr. **5** (1975) 483–491.
[4] A. Okubo, C. C. Ebbesmeyer, J. M. Helseth, *Determination of Lagrangian deformations from analysis of current followers*, J. Phys. Oceanogr. **6** (1976) 524–527.
[5] S. Petterssen, *On the relation between vorticity, deformation and divergence and the configuration of the pressure field*, Tellus **5** (1953) 231–237.

Exact solutions and short-wavelength instabilities for geophysical fluid flows

Delia Ionescu-Kruse

The study of geophysical fluid flows presents considerable challenges. Geometrical complexities, wind-driven surface waves, underlying non-uniform currents, density stratification, and so on, can occur. An in-depth qualitative study of the full problem is analytically intractable. In order to make the problem manageable, simplifying assumptions are formulated. For the wave-current interactions we rely on the inviscid theory. The Euler equations, the incompressibility condition and

the equation of mass conservation together with the appropriate kinematic and dynamic boundary conditions are written in a rotating frame with the origin at a point on the Earth's surface. The Earth is assumed to be a sphere of radius $\mathcal{R} = 6378$ km rotating eastward with a constant speed $\Omega = 73 \times 10^{-6}$ rad/s around its polar axis. Locally, it is convenient to use a Cartesian representation of the problem: at a latitude ϕ, we take a plane tangent to the surface of the Earth and a Cartesian coordinate system (x, y, z), the x-axis horizontally due east, the y-axis horizontally due north and the z-axis upward. In this coordinate system, the rotation vector $\mathbf{\Omega}$ has the components $(0, \Omega \cos \phi, \Omega \sin \phi)$. The Coriolis parameters, defined by $f := 2\Omega \sin \phi$, $\hat{f} := 2\Omega \cos \phi$, depend on the variable latitude ϕ. For surface water waves propagating zonally in a relatively narrow ocean strip less than a few degrees of latitude wide, it is adequate to use the f- or β-plane approximations [9, 11, 20]. Within the f-plane approximation, the Coriolis parameters are treated as constants, but within the β-plane approximation $\hat{f}$ is constant and a linear variation with the latitude is introduced, that is, $f + \beta y$, with f constant and $\beta := \frac{\hat{f}}{\mathcal{R}} = \frac{2\Omega \cos \phi}{\mathcal{R}}$; close to the Equator $\hat{f} = 2\Omega$, $f = 0$, $\beta = \frac{2\Omega}{\mathcal{R}}$. The approach pioneered by Gerstner of finding explicit exact solutions for gravity fluid flows within the Lagrangian framework, was extended to geophysical flows too. A Gerstner-like three-dimensional solution in the f-plane approximation at an arbitrary latitude, was obtained by Pollard [21]:

(1)
$$\begin{cases} x = x_0 - \frac{am}{k} e^{mz_0} \sin[k(x_0 - ct)] \\ y = y_0 + f\frac{am}{k^2 c} e^{mz_0} \cos[k(x_0 - ct)] \\ z = z_0 + a e^{mz_0} \cos[k(x_0 - ct)] \end{cases}$$

x_0, y_0, z_0 are the Lagrangian variables, $x_0 \in \mathbb{R}$, $y_0 \in \mathbb{R}$, $mz_0 \leq \tilde{z}_0 < 0$, $\tilde{z}_0$ being fixed, $k > 0$ is a fixed wave number, a, $m > 0$ are parameters and c is the wave speed. In order for the transformation (1) to be a local change of coordinates, the parameters a and m have to satisfy the condition $a^2 m^2 \leq 1$. From Euler's equations we also get $m^2(k^2 c^2 - f^2) = k^4 c^2$ and from the dynamical boundary condition we obtain the dispersion relation for the wave speed: $c^2(k^2 c^2 - f^2) = (g - \hat{f} c)^2$. The solution (1) is valid for arbitrary vertical stratification. In [8] a depth-invariant mean current was accommodated into (1). In the β-plane approximation, at an arbitrary latitude or in the equatorial region, nonlinear three-dimensional Gerstner-like solutions have also been derived (see, for example, [2, 3, 4, 12] and the references therein). For these solutions, the β-plane effect is not noticeable in the dispersion relation but manifests itself in the amplitude decay.

In the equatorial region, the underlying currents are highly depth-dependent: within the upper 200–250 m of the ocean there is a westward wind-driven current and a strong eastward jet, the Equatorial Undercurrent (EUC), at depths between 100-200 m [6, 9, 11]. The Gerstner-type exact solutions fail to capture strong depth-variations of the flows. Constantin & Johnson presented in [6] exact nonlinear solutions that describe equatorial flows on a rotating sphere with sufficient freedom, for example, arbitrary velocity profiles in the vertical direction, and are directly relevant to the EUC. The flows are described in a right handed spherical

coordinate system with the origin at a point on the Earth's surface, (r, θ, φ), $r > 0$, $0 \leq \theta = \frac{\pi}{2} - \phi \leq \pi$, $0 \leq \varphi \leq 2\pi$, with the unit vectors $(\mathbf{e}_r, \mathbf{e}_\theta, \mathbf{e}_\varphi)$. In this system, $\boldsymbol{\Omega} = \Omega \cos\theta \, \mathbf{e}_r - \Omega \sin\theta \, \mathbf{e}_\theta$, the velocity field $\mathbf{U} = U\mathbf{e}_r + V\mathbf{e}_\theta + W\mathbf{e}_\varphi$ and an exact steady solution to the free boundary problem, purely in the azimuthal direction, is given by [6]:

$$(2) \qquad\qquad U \;=\; 0 \;=\; V, \quad W \;=\; \mathcal{W}(r\sin\theta),$$

with $\mathcal{W}$ an arbitrary function of its argument. This function may be prescribed at the Equator for $\theta = \frac{\pi}{2}$. A simple choice for $\mathcal{W}(r)$ is the following parabolic profile:

$$(3) \qquad \mathcal{W}(r) = \begin{cases} W_e - (W_e + W_w)\left(\frac{r - \mathcal{R}_0}{\mathcal{R} - \mathcal{R}_0}\right)^2, & \text{for } \bar{\mathcal{R}} \leq r \leq \mathcal{R} \\ 0, & \text{for } r < \bar{\mathcal{R}} \end{cases}$$

where $\bar{\mathcal{R}} := \mathcal{R}_0 - (\mathcal{R} - \mathcal{R}_0)\sqrt{\frac{W_e}{W_e + W_w}}$, $W_w > 0$ is a constant surface speed to the West and $W_e > 0$ is a maximum constant speed at $r = \mathcal{R}_0 < \mathcal{R}$ within the EUC to the East. A similar approach [7] was successful for modeling the most significant current in our oceans and the only current that completely encircles the polar axis, that is, the Antarctic Circumpolar Current (ACC).

Once an exact solution is available, the study of its stability becomes an important issue. A rigorous mathematical approach to the problem of stability for general 3D inviscid incompressible flows is the short-wavelength method which was developed independently by Bayly [1], Friedlander & Vishik [10] and Lifschitz & Hameiri [19]. It turns out that this method is also successful for geophysical flows and geophysical barotropic flows, see the survey [16]. We disturb the rotating flow $(\mathbf{U}, P)$ by a small perturbation $(\mathbf{u}, p)$, with $\mathbf{u}_0$ at $t = 0$, P and p are the pressures. The evolution in time of small perturbations in the WKB form, that is, $\mathbf{u}(t, \mathcal{X}) = [\mathbf{A}(t, \mathcal{X}) + \epsilon\mathcal{A}(t, \mathcal{X})]\, e^{\frac{i}{\epsilon}\mathfrak{f}(t,\mathcal{X})} + \epsilon\mathbf{u}_{rem}(t, \mathcal{X}, \epsilon)$, $p(t, \mathcal{X}) = [B(t, \mathcal{X}) + \epsilon\mathcal{B}(t, \mathcal{X})]\, e^{\frac{i}{\epsilon}\mathfrak{f}(t,\mathcal{X})} + \epsilon p_{rem}(t, \mathcal{X}, \epsilon)$, ϵ a small parameter, $\mathcal{X}$ being either (x, y, z) or (r, θ, φ), is governed up to the remainder terms - terms that can be shown to be incapable of canceling the growth of the leading-order terms [13] - by the eikonal equation for the wave phase $\mathfrak{f}$ and the transport equation for the wave amplitude of the velocity $\mathbf{A}$. As the eikonal equation and the transport equation involve only the advective derivative along $\mathbf{U}$, we can think of this system of PDEs as a system of ODEs along trajectories of the the basic flow: $\frac{d\mathcal{X}}{dt} = \mathbf{U}(t, \mathcal{X})$. The local instability or stability depends on whether the amplitude vector $\mathbf{A}(t)$ grows with time or not. If for any initial data the amplitude vector $\mathbf{A}(t)$ is uniformly bounded in time, then the flow is stable, otherwise it is unstable. To detect instabilities, it is sufficient to make a clever choice for the initial position and direction of the wave vector that is likely to give an exponentially growing amplitude vector. For flows described in the Lagrangian framework, the usually nonlinear trajectories equations are already solved, thus, they are good candidates to apply the method.

Theorem 1 [14]. *If the Pollard waves* (1) *are sufficiently large, they are unstable; more precisely, if their steepness, defined as kae^{mz_0}, exceeds a specific threshold*

$$ake^{mz_0} > \frac{\sqrt{k^2c^2 - f^2}}{kc} \frac{\frac{k^2c^2 - 2f^2}{2kc\sqrt{k^2c^2 - f^2}} + \frac{\hat{f}}{kc}}{\sqrt{2 + \frac{2\hat{f}}{\sqrt{k^2c^2 - f^2}} + \left(\frac{k^2c^2 - 2f^2}{2kc\sqrt{k^2c^2 - f^2}} + \frac{\hat{f}}{kc}\right)^2}}$$

then, the amplitude $\boldsymbol{A}$ increases in time at an exponential growth rate.

For $f = 0$, $\hat{f} = 0$, the right-hand side becomes $\frac{1}{3}$, and we recover Leblanc's result [18] for Gerstner's wave. For equatorial waves, i. e. $f = 0$, $\hat{f} = 2\Omega$, the right-hand side has a value $\overset{>}{\approx} \frac{1}{3}$. For waves near the North Pole $f = 2\Omega$, $\hat{f} = 0$, the right-hand has a value $\overset{<}{\approx} \frac{1}{3}$ These considerations suggest that *the waves in polar regions are more prone to instability than those in the equatorial regions.*

A wave-steepness instability criterion for the Gerstner-like waves in the β-plane approximation, at an arbitrary latitude or at the Equator, can be also proved [2, 3, 5].

Theorem 2 [15], [17]. *For the exact steady flows purely in the azimuthal direction, the wave phase function $\mathfrak{f}$ is constant along the streamlines of the basic flow. The behavior in time of the amplitude vector $\mathbf{A}$ is determined by the eigenvalues of the matrix of an autonomous linear differential system. For some realistic velocity profiles relevant for the EUC model (for example, (3)) or for the ACC model, $\mathbf{A}$ remains bounded in time, thus, these flows are locally stable.*

REFERENCES

[1] B. J. Bayly, *Three-dimensional instabilities in quasi-two dimensional inviscid flows*, Nonlinear wave Interactions in fluids (ed. R. W. Miksad et al.), 71–77, ASME, New York, 1987.

[2] J. Chu, D. Ionescu-Kruse, Y. Yang, *Exact solution and instability for geophysical waves at arbitrary latitude*, Disc. Cont. Dyn. Syst. **39** (2019), 4399–4414.

[3] J. Chu, D. Ionescu-Kruse, Y. Yang, *Exact solution and instability for geophysical waves with centripetal forces at arbitrary latitude*, J. Math. Fluid Mech.**21** (2019), Art. No.: UNSP 19.

[4] A. Constantin, *An exact solution for equatorially trapped waves*, J. Geophys. Res.**117** (2012), C05029.

[5] A. Constantin, P. Germain, *Instability of some equatorially trapped waves*, J. Geophys. Res.-Oceans **118** (2013), 2802–2810.

[6] A. Constantin, R. S. Johnson, *An exact, steady, purely azimuthal equatorial flow with a free surface*, J. Phys. Oceanogr. **46** (2016), 1935–1945.

[7] A. Constantin, R. S. Johnson, *An exact, steady, purely azimuthal flow as a model for the Antarctic Circumpolar Current*, J. Phys. Oceanogr. **46** (2016), 3585–3594.

[8] A. Constantin, S. G. Monismith, Gerstner waves in the presence of mean currents and rotation, *J. Fluid Mech.* **820** (2017), 511-528.

[9] B. Cushman-Roisin, J. M. Beckers, "Introduction to Geophysical Fluid Dynamics: Physical and Numerical Aspects", Academic, Waltham, Mass., 2011.

[10] S. Friedlander, M. M. Vishik, *Instability criteria for the flow of an inviscid incompressible fluid*, Phys. Rev. Lett. **66** (1991), 2204–2206.

[11] A. E. Gill, "Atmosphere-Ocean Dynamics", Academic, 1982.

[12] D. Henry, *On three-dimensional Gerstner-like equatorial water waves*, Philos. Trans. Roy. Soc. A **376** (2018), no. 2111, 20170088, 16 pp.

[13] D. Ionescu-Kruse, *Instability of equatorially trapped waves in stratified water*, Ann. Mat. Pura Appl. **195** (2016), 585–599.

[14] D. Ionescu-Kruse, *Instability of Pollard's exact solution for geophysical ocean flows*, Physics of Fluids **28** (2016), no.086601.

[15] D. Ionescu-Kruse, *Local stability for an exact steady purely azimuthal flow which models the Antarctic Circumpolar Current*, J. Math. Fluid Mech. **20** (2018), 569–579.

[16] D. Ionescu-Kruse, *On the short-wavelength stabilities of some geophysical flows*, Philos. Trans. R. Soc. A **376** (2018), 20170090.

[17] D. Ionescu-Kruse, C. I. Martin, *Local Stability for an Exact Steady Purely Azimuthal Equatorial Flow*, J. Math. Fluid Mech. **20** (2018), 27–34.

[18] S. Leblanc, *Local stability of Gerstner's waves*, J. Fluid Mech. **506** (2004), 245–254.

[19] A. Lifschitz, E. Hameiri, *Local stability conditions in fluid dynamics.*, Phys. Fluids **3** (1991), 2644—2651.

[20] J. Pedlosky, "Geophysical Fluid Dynamics, Springer, New York, 1979.

[21] R. T. Pollard, *Surface waves with rotation: An exact solution*, J. Geophys. Res. **75** (1970), 5895–5898.

Non-radial kernel-based interpolation for the sphere

JANIN JÄGER

(joint work with Martin Buhmann, Jean Carlo Guella)

Strictly positive definite kernels $K : \mathbb{S}^{d-1} \times \mathbb{S}^{d-1} \to \mathbb{C}$, allow the unique solution of the following interpolation problem:

Let $\Xi \subset \mathbb{S}^{d-1}$ be a finite set of distinct points, and $f(\xi) \in \mathbb{C}$, $\xi \in \Xi$, a set of function values. Find $s : \mathbb{S}^{d-1} \to \mathbb{C}$ satisfying

$$s(\zeta) = \sum_{\xi \in \Xi} \lambda_\xi K(\xi, \zeta) = f(\zeta), \quad \forall \zeta \in \Xi,$$

$\lambda_\xi \in \mathbb{C}$.

These kernels are not necessarily radially symmetric but the isotropic kernels (or spherical radial basis functions), for which the value of K only depends on the geodesic distance between its arguments, are a subset of this class. There are only few results on this class of kernels if radial symmetry is not assumed.

We use the series expansion of the kernel in spherical harmonics to give a general representation of such kernels without assuming radial symmetry, before we study kernels with specific (weaker) properties like axial symmetry or invariance under parity. For kernels with these properties we derive conditions that ensure (strict) positive definiteness.

Simulating ocean eddies: Parameterizations and diagnostics

STEPHAN JURICKE

We present and diagnose a set of new momentum closures that can help to substantially reduce overdissipation in global ocean simulations. In this context, a good representation of mesoscale turbulence is crucial for realistic simulations of the major ocean currents, their variability, and overall ocean dynamics. The choice of momentum closures can strongly affect the representation of mesoscale turbulence. Generally, ocean models at resolutions close to or slightly finer than the Rossby radius of deformation are too dissipative, killing both existing eddies as well as preventing the formation of sufficiently many new eddies.

We discuss our implementation of the kinetic energy backscatter parameterization which works in combination with a classical viscous closure. It generally reinjects energy with an anti-dissipative operator that acts on larger scales than the viscous operator. It therefore reinjects energy at larger scales then those smaller scales that are strongly affected by viscous dissipation. The combination of both leads to a numerically stable, energized flow simulation that is substantially less dissipative than a purely viscous closure. Different methods for choosing the amplitude of local backscatter and the form of the backscatter operator as well as different viscosities are discussed. All simulations have been carried out with the unstructured grid, finite volume ocean model FESOM2. We adapt the spectral diagnostics for energy and dissipation power to be able to use them on the triangular grids utilized by FESOM2.

The main conclusions are that the backscatter parameterizations are able to re-energize the flow and substantially improve simulations of the global ocean circulation as well as the stratification. However, they need to be carefully constrained to achieve best results. Various backscatter options exist in FESOM2; not all adapt automatically with resolution. Finally, suitable (spectral or alternative scale) diagnostics for scale interactions on unstructured grids are crucial to understand associated energy transfers.

Deterministic and stochastic surrogate models for fast oscillatory motion

MARC AURELE TIOFACK KENFACK
(joint work with Marcel Oliver)

Spontaneous generation is one of the mechanisms by which gravity waves are generated from atmospheric or ocean models. It has the fundamental implications that it limits the validity of balanced models and provides the sources of gravity wave activity. It's therefore directly linked to the problem of dynamical regimes (slow and fast dynamics) separation in geophysical flows, which has a non-negligible role in numerical weather predictions. In this work, we describe this phenomenon in an idealized setting, but from a slightly broad point of view by providing a model based on the asymptotic estimate of the amplitude of waves generated,

which substitutes very accurately the parent system in the generation of unbalanced dynamics. The Lorenz'63 system is used as a generator of pseudo-random or periodic sequences of poles, the latter being detected by using the AAA algorithm for rational interpolation. The surrogate model is corroborated via the 0-1 test for chaos by [1, 2] and highlights the crucial role that plays the phase of the singularities of the system.

REFERENCES

[1] Gottwald, G. A. and Melbourne, I. (2004). A new test for chaos in deterministic systems. Proceedings of the Royal Society of London. Series A: Mathematical, Physical and Engineering Sciences, 460(2042):603–611.
[2] Gottwald, G. A. and Melbourne, I. (2016). The 0-1 test for chaos: A review. Chaos detection and predictability, pages 221–247.

Thoughts on Machine Learning

RUPERT KLEIN

Concerns: Techniques of machine learning (ML) and what is called "artificial intelligence" (AI) today find a rapidly increasing range of applications touching upon social, economic, and technological aspects of everyday life. They are also being used increasingly and with great enthusiasm to fill in gaps in our scientific knowledge by data-based modeling approaches. I have followed these developments over the past almost 20 years with interest and concern, and with mounting disappointment. This leaves me sufficiently worried to raise here a couple of pointed remarks.

Obviously, when these technologies are being employed to take over decisive functionality in safety-critical applications, we would like to exactly know how to guarantee their compliance with pre-defined guardrails and limitations. Moreover, when ML techniques are utilized as building blocks in scientific research, it would violate scientific standards – in the authors opinion – if these building blocks were used without a thorough understanding of their functionality, including inaccuracies, uncertainties, and other pitfalls.

The most frequently used tools in ML and AI today are deep neural networks (DNNs) and, to the best of my knowledge, they currently constitute a particularly severe breach of what I postulate to be desirable for safety-critical applications and for their utilization in scientific research. In fact, I see the following related and further drawbacks:

a) Interpretability/Explainability: It is remarkable that the issue of how to reliably interpret the workings of DNN technology has become a topic of intense research only relatively recently, see [1], and can by far not be considered fully explored today.

b) Generalizability and out-of-sample performance: The quality of ML-learned functions is quite usually tested via some version of cross-validation [2]: Split the available data into a training and one or more testing sets, train the

function on the former and test "generalizability" utilizing the latter. A key problem with the often rather high-dimensional spaces of function arguments is that no explicit definition of the domain of the learned function is provided. Therefore, when a new input argument is to be used in an application, there seem to be no systematic qualifiers that would indicate whether this argument may or may not be used as an argument of the learned function with any confidence.

c) Inefficiency in terms of data needed: DNNs are "big data" techniques, and it turns out they do, in fact, need rather large data sets for training – with consequences for the computational expense of their training, [3].

d) Inefficiency of function representation: DNNs based on ReLU (rectified linear unit) activation functions are popular in AI generically and as building blocks of more complex function constructions. ReLU-DNNs are known to represent piecewise linear functions on polygones in the space of function arguments, and He et al. [4] show that ReLU-DNNs require on the order of $D\kappa^D N$ free parameters to represent a piecewise linear function on a simplicial grid with N nodes in D dimensions, with $\kappa \geq 2$. Comparing this, for large D, with the number of degrees of freedom needed for the same task by a standard finite element ansatz, i.e., with $(D+1)N$, we find another reason for the extensive computational costs of DNN training.

e) Inefficiency of optimization algorithms: Thus far, (variants of) stochastic gradient descent methods for the solution of the DNN parameter estimation problem seem to be essentially the only reliable option [5]. Yet, these come with at most first order convergence, with further consequences for the computational expense of DNN training in comparison with methods the structure of which allows employing second order convergent Newton-type techniques in solving their parameter estimation problem.

f) Condition / Sensitivity: A mounting number of examples in the literature show that ML-learned functions can be tricked by so-called "adversarial attacks" to yield clearly false or low-quality results by effectively exploiting the often bad conditioning of the function learning problem, see [6, 7, 8, 9] and references therein.

Alternatives: We are not bound to utilizing neural network technology for machine learning and in the context of artificial intelligence, however. Alternatives that overcome many of the above mentioned drawbacks and limitations are being developed. In this context, I have become aware of the recent family of "Sparse Probabilistic Approximations" (SPA) [3, 10, 11, 13] by Illia Horenko and co-workers. These methods turn out to be (i) at least as – and in many cases much more – powerful than DNNs in terms of the quality of functions learned; they (ii) come with natural indicators for the domain of the learned functions; targeting *small data problems* by design, they are (iii) generically much less data hungry than DNNs (thereby avoiding concern c), see above); their parameter estimation

can (iv) be cast into optimization problems that are amenable to far-reaching partially analytical and iterative methods yielding second-order convergence; versions are available that (v) address a wide range of ML tasks, such as clustering, classification, regression, and more. On problems it has been used for, such as cancer classification, data-based El Niño prediction, or financial decision making [12], the recent eSPA+[1] technique for data classification in [13] has out-performed DNNs and other machine learning techniques decisively in terms of the quality of results or computational efficiency or both. As regards computational efficiency, the method comes with complexity $T \cdot D \cdot K$, where, T, is the number of available data samples, D is dimension of the function argument (or feature) space, and K is akin to the number of allowed input data clusters one would impose when applying some clustering technique for dimension reduction. In fact, this complexity is that of the K-means clustering algorithm, which is highly efficient but all by itself insufficient to solve machine learning problems beyond data clustering.

As is the case for the entire SPA family of methods, eSPA+ comes with a clean mathematical structure in which each ingredient has a transparent role and interpretation. This is seen in the following example: The parameter estimation problem of eSPA+ for the El Niño prediction problem reads as

$$
(1) \qquad (S, \Gamma, W, \Lambda)^\circ = \operatorname*{argmin}_{\boldsymbol{S}, \boldsymbol{\Gamma}, \boldsymbol{W}, \boldsymbol{\Lambda}} \mathcal{L}^+_{\mathrm{eSPA}} \left(\boldsymbol{S}, \boldsymbol{\Gamma}, \boldsymbol{W}, \boldsymbol{\Lambda} \mid \boldsymbol{X}, \boldsymbol{\Pi}^{\Delta t} \right) .
$$

Here $\boldsymbol{X} = (X_t)_{t=1}^T \in \boldsymbol{R}^{D \times T}$ is the set of D-dimensional function arguments in the available data set. In the example, each $X_t \in \boldsymbol{R}^D$ consists of $D = 200$ degrees of freedom characterizing tropical pacific ocean sea surface and equatorial deep ocean water temperatures. $\boldsymbol{\Pi}^{\Delta t} = (\Pi_t^{\Delta t})_{t=1}^T \in \{0, 1\}^T$ is the set of observations stating whether at time $t + \Delta t$ an El Niño did ($\Pi_t^{\Delta t} = 1$) or did not ($\Pi_t^{\Delta t} = 0$) occur; $\boldsymbol{S} \in \boldsymbol{R}^{D \times K}$ is a matrix whose columns $S_k \in \boldsymbol{R}^D$ are K centers of data clusters or "boxes" in the space of function arguments akin to cluster centers in the K-means scheme, and $\boldsymbol{\Gamma} \in [0, 1]^{K \times T}$ is a columnwise probabilistic matrix such that, when the problem has been solved, $(S^\circ \Gamma^\circ)_t \approx X_t$ provides a reduced approximate representation of the argument-space input data $\boldsymbol{X}$; $\boldsymbol{W} \in [0, 1]^D$ is a probability distribution over the dimensions of the argument (or feature) space with small W_d indicating weak influence of the dth data dimension on the prediction outcome, and $\boldsymbol{\Lambda} \in [0, 1]^K$ is the set of probabilities Λ_k of El Niño occuring a time of Δt down the road if a data point belongs to the kth cluster.

---

[1]eSPA+ = entropy-optimal scalable probabilistic approximation, with algorithmic efficiency enhancements

The functional to be minimized then reads as

$$\mathcal{L}^*_{\mathrm{eSPA}}\left(\boldsymbol{S}, \boldsymbol{\Gamma}, \boldsymbol{W}, \boldsymbol{\Lambda} \mid \boldsymbol{X}, \boldsymbol{\Pi}^{\Delta t}\right) = \underbrace{\frac{1}{T}\sum_{d=1}^{D} W_d \sum_{t=1}^{T} (X_{d,t} - (S\Gamma)_{d,t})^2}_{D\text{-red.: state approximation error}}$$

(2)

$$- \underbrace{\varepsilon_W \sum_{d=1}^{D} W_d \log\left(\frac{1}{W_d}\right)}_{D\text{-red.: feature discrimination}} - \underbrace{\frac{\varepsilon_\Lambda}{T}\sum_{t=1}^{T} \Pi_t^{\Delta t} (\ln(\Lambda)\,\Gamma)_t}_{\text{supervision}}.$$

All terms in this functional have a clear interpretation: The first term on the right is a W-weighted Euclidean norm measuring the quality of approximating $\boldsymbol{X}$ by $(\boldsymbol{S\Gamma})$. The role of this term is to enable an effective dimension reduction in that the key information in the space of arguments is stored in the K reference points (or cluster centers) S_k°, with $K \ll T$ when the approach is successful. The dimension-wise weighting by W_d of the components $(X_{d,t} - (S\Gamma)_{d,t})^2$ of the Euclidean distance enables a further effective dimension reduction in that dimensions (or features) that only minimally affect the El Niño prediction receive a lesser weight in the solution and therefore contribute only marginally to the functional's value when the problem is solved. To achieve a least-biased discrimination of features in this way, the Shannon entropy of the distribution $\boldsymbol{W}$ is subtracted from the functional as a penalty in the second term on the right. That is, we seek to maximize Shannon-entropy and thus find the broadest possible distribution $\boldsymbol{W}$ under the given conditions.

The third term on the right, which implements the supervision of the classification learning problem, stems from interpreting the data $\Pi_t^{\Delta t} \in \{0,1\}$ as probabilities for the occurrence of El Niño some time Δt in the future, and then

$$(3) \qquad -\sum_{t=1}^{T} \Pi_t^{\Delta t} (\ln(\Lambda)\,\Gamma)_t \approx \sum_{t=1}^{T} \Pi_t^{\Delta t} \ln\left(\frac{1}{(\Lambda\Gamma)_t}\right)$$

is an approximation to that part of the Kullback-Leibler (KL) divergence between the data $\Pi_t^{\Delta t}$ and their approximations $(\boldsymbol{\Lambda\Gamma})_t$ which depends explicitly on the unknowns $\boldsymbol{\Lambda}$ and $\boldsymbol{\Gamma}$. It turns out that this latter approximation provably generates an upper bound for the functional utilizing the original KL-divergence, and in this sense the approximation is robust.

Now, once we have $(\boldsymbol{S}, \boldsymbol{\Gamma}, \boldsymbol{W}, \boldsymbol{\Lambda})^\circ$ determined by solving the above minimization problem, and today's state of ocean temperature data X^* is observed, then a probabilistic El Niño forecast is obtained as follows: Find the best-possible approximation of X^* by a convex combination $\boldsymbol{S}\Gamma^*$ of the reference points S_k, with $\Gamma^* \in [0,1]^K$, $\sum_{k=1}^{K} \Gamma_k^* = 1$. This yields the pertinent probabilistic weights Γ_k^* and the eSPA+-predicted probability for El Niño occurance a time Δt from today becomes $\Lambda\Gamma^* = \sum_{k=1}^{K} \Lambda_k \Gamma_k^*$.

Besides the clear interpretability of this method (concern a) taken care of), there is also an exceedingly efficient algorithm for its training: The idea detailed in [13]

is to iteratively solve for one of the unknowns in $(\boldsymbol{S}, \boldsymbol{\Gamma}, \boldsymbol{W}, \boldsymbol{\Lambda})$ while keeping the other three fixed. Each of these steps allows for either an analytical or a numerical solution that scales linearly in the complexity parameters (D, T, K), and the entire iteration procedure can be cast as a Newton-type method [14]. This yields very fast (second order) convergence, so that concern e) does not arise for the SPA-family of methods.

Note also, that the convex hull of the reference points S_k° serves as a natural and robust estimate of the domain of the learned function. Thus, concern b) would at least in part be taken care of as well.

As regards concern d), it is shown in [3, 10] that the variant of eSPA+ described in (1)–(3) produces piecewise linear solutions on simplices with corners defined by the references points S_k. Therefore, these solutions are classical linear finite element functions, and the number of degrees of freedom needed to represent them is $(D+1)K$. Hence, eSPA+ does not suffer from concern d) either.

Addressing the remaining robustness concern f) for the SPA-family of methods is work in progress at the time of this writing.

References

[1] https://de.wikipedia.org/wiki/Explainable_Artificial_Intelligence
[2] https://en.wikipedia.org/wiki/Cross-validation_(statistics)
[3] I. Horenko, *On a Scalable Entropic Breaching of the Overfitting Barrier for Small Data Problems in Machine Learning*, Neural Comput., **32**, 1563–1579 (2020)
[4] J. He, L. Li, J. Xu, Ch. Zheng, *ReLU deep neural networks and linear finite elements*, J. Comput. Math., **38**:3, 502–527 (2020)
[5] St.J. Wright, B. Recht, *Opitimzation for data analysis*, Cambridge University Press (2022), https://doi.org/10.1017/9781009004282
[6] https://openai.com/research/attacking-machine-learning-with-adversarial-examples
[7] Z. Klawikowska, A. Mikołajczyk, M. Grochowski, *Explainable AI for Inspecting Adversarial Attacks on Deep Neural Networks*, in: L. Rutkowski et al. (Eds.), ICAISC 2020, LNAI 12463, pp. 134–146, 2020.
[8] B. Dickson, https://bdtechtalks.com/2020/12/16/machine-learning-adversarial-attacks-against-machine-learning-time-bomb/ (original) https://www.kdnuggets.com/2021/01/machine-learning-adversarial-attacks.html (re-post)
[9] N. Akhtar, A. Mian, N. Kardan, M. SHAH, *Advances in Adversarial Attacks and Defenses in Computer Vision: A Survey*, IEEE Access, **9**, 155161–155196
[10] S. Gerber, L. Pospisil, M. Navandar, I. Horenko, *Low-cost scalable discretization, prediction, and feature selection for complex systems*, Sci. Adv., **6**:5, eaaw0961 (2020)
[11] I. Horenko, *Scalable Entropy-Optimal Machine Learning Classification for Small Data Problems*, PNAS, **119**:9, e2119659119 (2022)
[12] E. Vecchi, *Efficient and scalable solution techniques for small data learning problems*, Dissertation, Faculty of Informatics, Università della Svizzera Italiana, Lugano (2023)
[13] E. Vecchi, L. Pospisil, S. Albrecht, T.J. O'Kane, I. Horenko, *Scalable Entropy-Optimal Machine Learning Classification for Small Data Problems*, Neural Comput., **34**:5, 1220–1255 (2022)
[14] I. Horenko, E. Vecchi, J. Kardoš, Andreas Wächter, Olaf Schenk, Terence O'Kane, Patrick Gagliardini, Susanne Gerber, *On cheap entropy-sparsified regression learning*, PNAS, **120**:1, e2214972120 (2023)

Lagrangian Coherent Structures for describing ocean transport across scales: from the large scale circulation to the sub-mesoscale

Ana M. Mancho

Following the spirit of Poincarś works, which identify geometrical partitions in the phase space that separate solutions of dynamical systems with qualitatively different behaviors, in the context of geophysical flows, Lagrangian Coherent Structures (LCS) are structures that recognize regions where fluid trajectories have different origins or fates. Indeed, in the purely advective approach, fluid parcels evolve according to the dynamical system:

$$(1) \qquad \frac{d\mathbf{x}}{dt} = \mathbf{v}(\mathbf{x}, t),$$

where $\mathbf{v}(\mathbf{x}, t)$ is the vector field, linked to the ocean velocity field. In this setting, Lagrangian Coherent Structures can be used to study transport, and events ranging from global-scale circulation to sub-mesoscale coastal applications are reported. In these applications, LCS are computed with the tool of Lagrangian Descriptors introduced in [1, 2, 3].

First, recent results reported in [4] on ocean transport across the global Atlantic Meridional Overturning Circulation (AMOC) are discussed. The results explore transport across a climatological model for the AMOC in which the velocity field in Eq. (1) is obtained from averages of velocities of the ECCO product [5] over many years (1992-2017). This leads to a 3D stationary dynamical system (the averaged velocity does not depend on time), where vertical transport is studied with the support of LCS. The discussion is focused on two regions. The first one is the Flemish Cap region, a zone of interaction between the major AMOC components. Here, the analysis identifies a domain of deep waters that ascend very rapidly to the ocean surface, in just 80 days. The second region is the Irminger Sea. Here, the analysis confirms the existence of a downwelling zone and reveals a previously unreported upwelling connection between very deep waters and the ocean surface, where waters slowly ascend in a swirling manner in around 800 days.

The second application discusses results reported in [6] on the ability of LCS to characterize a spill produced in Gran Canaria after the crash of the ferry Volcan Tamasite with the Mandela Pier of the Port of La Luz on Friday, 21st April 2017. In this setting, LCS have provided a deep understanding of the dispersion produced by ocean currents as they identify key dynamical objects controlling transport in the area. In particular, hyperbolic trajectories are attached to the coastline in a detachment configuration. This kind of hyperbolic trajectories has the unstable manifold transversal to the coast. Under the presence of this dynamical object, the spill evolves, leaving the coast towards the interior of the ocean, becoming aligned with the unstable manifold. Satellite and in situ observations are consistent with the existence of this dynamical structure, which is found in both a very high-resolution model (at a metric scale) for La Luz Port, produced by Puertos del Estado, and in a coarser dataset available from the Copernicus Marine Environmental Monitoring Service (CMEMS) for the Iberia-Biscay-Ireland domain.

The attempt to compare the performance of each model in this event, with respect to the observed evolution of the spill, leads to a measure of the error, for which a spatial structure is found closely connected to the *stable manifolds* of the hyperbolic trajectories present in the dynamical system (1). These connections are thoroughly explored in [7]. More recently, the analysis of an oil spill of unknown origin affecting the coast of Israel in 2021 [8] has allowed further exploration of correspondences between the uncertainty associated with specific datasets regarding the observations and the *unstable manifolds* of the hyperbolic trajectories present in the dynamical system (1) (see [9]).

References

[1] C. Mendoza, A. M. Mancho, *The hidden geometry of ocean flows*, Phys. Rev. Lett., **105** (2010), 038501.

[2] A. M. Mancho, S. Wiggins, J. Curbelo, C. Mendoza, *Lagrangian descriptors: A method for revealing phase space structures of general time dependent dynamical systems*, Communications in Nonlinear Science and Numerical Simulations, **18** (2013), 3530-3557.

[3] C. Lopesino, F. Balibrea-Iniesta, V. J. García-Garrido, S. Wiggins, A. M. Mancho, *A theoretical framework for Lagrangian Descriptors*, International Journal of Bifurcation and Chaos, **27** (2017), 1730001.

[4] R. Bruera, J. Curbelo, G. Garcia-Sanchez, A.M. Mancho, *Mixing and Geometry in the North Atlantic Meridional Overturning Circulation*, Geophysical Research Letters **50** (2023), e2022GL102244.

[5] ECCO Consortium, Fukumori, I., Wang, O., Fenty, I., Forget, G., Heimbach, P.,Ponte, R. M. *ECCO Central Estimate (Version 4 Release 4).394 ecco.jpl.nasa.gov/drive/files/Version4/Release4/interp_113monthly.395 ([Online; accessed July-2021])* (2021).

[6] G. García-Sánchez, A. M. Mancho, A. G. Ramos, J. Coca, B. Pérez-Gómez, E. Álvarez-Fanjul, M. G. Sotillo, M. García-León, V. J. García-Garrido, S. Wiggins, *Very High Resolution Tools for the Monitoring and Assessment of Environmental Hazards in Coastal Areas*, Frontiers in Marine Science **7** (2021), 605804.

[7] G. García-Sánchez, A. M. Mancho, S. Wiggins, *A bridge between invariant dynamical structures and uncertainty quantification*, Commun. Nonlinear Sci. Numer. Simul. **104** (2022), 106016.

[8] G. García-Sánchez, A. M. Mancho, A. G. Ramos, J. Coca, S. Wiggins, *Structured pathways in the turbulence organizing recent oil spill events in the Eastern Mediterranean* , Scientific Reports **12** (2022), 3662.

[9] G. García-Sánchez, A. M. Mancho, M. Agaoglou, S. Wiggins, *New links between invariant dynamical structures and uncertainty quantification*, Physica D. **453** (2023), 133826.

Buoyant Clustering and Reactivity of Ocean Contaminants.

Jamie Meacham

(joint work with Pavel Berloff)

Accurate modeling of mixing processes in the ocean is essential to understanding the ecological risk posed by contaminants such as plastic pollutants and agricultural runoff. Observations of floating material at the ocean surface, such as microplastic pollutants, as well as biological populations like phytoplankton [1] and Sargassum [2] show a tendency to form dense clusters. One mechanism behind this is that particles with neutral/positive buoyancy behave in a fundamentally different way to passive tracers. In particular, buoyant particles have a tendency to form a layer around the vertical level of their neutral buoyancy [3]. As a result, they predominantly follow the horizontal surface currents, which are weakly convergent.

We construct an idealized model of floating tracers where particles follow a kinematic ocean surface velocity and couple this to a simple biogeochemical model representing reactions between nutrients (which follow the full 3-dimensional flow passively), buoyant plankton and buoyant contaminants.

Cluster formation by buoyancy forces are found to significantly alter the long-time behavior of the system. An analytic expression for the new equilibrium is derived and verified with numerical experiments. We find that contaminants are far more potent when clustering occurs, due to efficient mixing between them and the plankton population. The new equilibrium is characterized by a sharp cutoff for plankton extinction, with extinction occurring at a much lower rate of contaminant forcing.

References

[1] A. Jordi, G. Basterretxea, S. Anglès, *Influence of ocean circulation on phytoplankton biomass distribution in the Balearic Sea: Study based on Sea-viewing Wide Field-of-view Sensor and altimetry satellite data*, J. Geophys. Res. **114** (2009), C11005.

[2] J. Gower, C. Hu, G. Borstad, S. King, *Ocean Color Satellites Show Extensive Lines of Floating Sargassum in the Gulf of Mexico*, IEEE Transactions on Geoscience and Remote Sensing **44** (2006) 3619-3625

[3] C. Reartes, P.D. Mininni, *Dynamical regimes and clustering of small neutrally buoyant inertial particles in stably stratified turbulence*, Phys. Rev. Fluids **8** (2023), 054501.

Report on work relating to Sampling-Dependent Transition Paths of Iceland–Scotland Overflow Water

Philippe Miron

Recently introduced in oceanography to interpret the near-surface circulation, transition path theory (TPT) is a methodology that rigorously characterizes ensembles of trajectory pieces flowing out from a source last and into a target next, i.e., those that most productively contribute to transport. As part of two recent publications, we used TPT to study the deep circulation of the North Atlantic

ocean, and quantify the different pathways out of the region. Transition path theory (TPT) based on Markov chains has been applied to investigate the equatorward export of Iceland-Scotland Overflow Water (ISOW). Previous analysis of trajectories of submerged floats challenged the conventional theory of abyssal circulation, which posits that ISOW should flow steadily along a deep boundary current (DBC) around the subpolar North Atlantic before exiting.

The TPT analysis focuses on the flow from the origin of ISOW to its exit region in the subpolar North Atlantic and suggests that insufficient sampling may introduce bias into previous conclusions. Three time-homogeneous Markov chains are constructed to model ISOW flow: one with a high number of simulated trajectories covering the flow domain uniformly, and two with fewer trajectories that cover the domain heterogeneously, using observed or simulated trajectories subsampled at the observed frequency. The densely sampled chain supports a well-defined DBC, although it is uncertain if this is specific to the considered simulation. However, the more heterogeneously sampled chains, regardless of the nature of trajectories used, do not exhibit a clear DBC. Analyzing the sensitivity of the Markov chains to sampling, recommendations are made to expand the existing float dataset for improved accuracy in drawing conclusions about long-term aspects of ISOW circulation.

REFERENCES

[1] F.J. Beron-Vera, M.J. Olascoaga, L. Helfmann and P. Miron, *Sampling-Dependent Transition Paths of Iceland–Scotland Overflow Water*, Journal of Physical Oceanography **53** (2022), 1151–1160.
[2] P. Miron, F.J. Beron-Vera and M.J. Olascoaga, *Transition paths of North Atlantic Deep Water*, Journal of Atmospheric and Oceanic Technology **39** (2022), 959–971.

Stepsize Variations for Lyapunov Exponents to Counter Persistent Errors

FLORIAN NOETHEN

Lyapunov exponents are important quantities in the analysis of complex dynamical systems. Usually, they are computed with Benettin's algorithm, which propagates linear perturbations along a background trajectory. While many applications trust in convergence of the algorithm, they often do not consider the effects of numerical errors. In fact, integration errors tend to accumulate in the averaging process of Benettin's algorithm when using constant or adaptive stepsizes and lead to limits different from the Lyapunov exponents.

I will present rules for stepsizes to counter the accumulation of integration errors. Rigorous convergence results are obtained for a broad class of linear systems while numerical observations indicate similar behavior for nonlinear systems [1]. Finally, I will discuss ideas on how to extend the convergence results from linear to nonlinear systems via Koopman theory.

REFERENCES

[1] F. Noethen, *Stepsize Variations for Lyapunov Exponents to Counter Persistent Errors*, (2023) arXiv:2112.11388v2.

Inertial ocean dynamics

MARIA J. OLASCOAGA

(joint work with F.J. Beron-Vera and P. Miron)

It has been long observed in fluid mechanics that finite-size, buoyant or *inertial* particle motion differs from infinitesimally small, neutrally buoyant or Lagrangian particle motion. The seminal work of Maxey and Riley in 1983 [1] established first principles foundation for this observation, representing the result of many years of research starting with the pioneering study of Sir George Stokes in the mid 1800s on the motion of a small solid sphere (pendulum) immersed in a fluid at rest.

The *Maxey–Riley equation* is a Newton-type second law involving several forces. These included, mainly, the *flow force* (exerted on the particle by the undisturbed fluid), the *added mass force* (resulting from the part of the fluid moving with the particle), the *lift force* (arising when the particle rotates as it moves in a sheared flow), and the *Stokes drag* (caused by the fluid viscosity).

The Maxey–Riley equation represents an undisputed framework for the study of inertial particle motion in fluid mechanics. However, efforts by the *geophysical* fluid dynamics community to adopt the Maxey–Riley framework are scarce, including a handful of applications in meteorology and oceanography.

The portability of the Maxey–Riley equation to oceanography has been thwarted by the challenging problem of accounting for the combined effects of ocean currents *and* winds on particle drift. This problem, which has been approached in a largely piecemeal ad-hoc manner in oceanohraphy, was addressed recently by Beron-Vera, Olascoaga and Miron [2]. These authors derived from the Maxey–Riley equation a new equation—referred to herein as the *BOM equation*—for the drift of inertial particles *floating at the air–sea interface*.

More specifically, the derivation of the BOM equation starts by considering a small spherical particle floating at the interface between two homogeneous fluids. The heavier fluid represents the ocean water. The (much) lighter fluid atop represents the air. The BOM equation follows by vertically integrating the Maxey–Riley equation across the particle's extent. An important addition in the geophysical case is the *Coriolis force*, which is the only perceptible effect of the planet's rotation in a frame attached to the planet such that the local vertical is sufficiently tilted toward the nearest pole to counterbalance the centrifugal force.

As with the Maxey–Riley equation, the positions of the particles in the BOM equation evolve slowly in time while their velocities vary rapidly. This makes the BOM equation a singular perturbation problem. Geometric singular perturbation theory can then be applied to study the long-time asymptotic nonlinear dynamics of inertial particles on the *slow manifold*, M_τ, which attracts all the solutions of the BOM equation exponentially fast in time.

More specifically, unique up to an error of $O(e^{-1/\tau}) \ll O(\tau)$, the locally invariant slow manifold M_τ normally attracts all solutions of the BOM equation when $\tau > 0$ is small exponentially fast (Fig.1). Proportional to the square of the particle radius, τ is the Stokes time, setting the inertial particle's response time to the medium. The manifold M_τ lies $O(\tau)$-close to the critical manifold, M_0. For the fast dynamics, i.e., with time rescaled by τ^{-1}, M_0 is filled with fixed points, while for the slow dynamics, i.e., with time unscaled, motion on M_0 is nontrivial, evolving according to the *buoyancy-weighted average of water (v) and air (w) velocities*, viz.,

$$(1) \qquad u(x,t) = (1-\alpha)v(x,t) + \alpha w(x,t)$$

where x stands for horizontal position, t is time, and $\alpha > 0$ is a (typically very small) parameter that depends on the water-particle-density ratio ($\delta > 1$) in closed form, known as *windage*. With and $O(\tau^2)$-error, the *reduced BOM equation*

$$(2) \quad \dot{x} = u + \tau u_\tau, \quad u_\tau := \left(R\frac{Dv}{Dt} + R\left(f + \tfrac{1}{3}\omega\right)v^\perp - \frac{Du}{Dt} - \left(f + \tfrac{1}{3}R\omega\right)u^\perp\right)$$

controls the motion off M_τ. Here, $\omega := \nabla \cdot v^\perp$ is the vorticity, $R > 0$ is a function of δ (decaying from 1), and f is the Coriolis parameter. When $\tau = 0$, each point off M_0 belongs to the stable manifold of M_0, which is foliated by its distinct stable fibers (stable manifolds of points on M_0). The stable manifolds of M_0 and its stable fibers perturb along with M_0. Consequently, for $0 < \tau \ll 1$ each point off M_τ is connected to a point on M_τ by a fiber in the sense that is follows a trajectory that approaches its partner on M_τ exponentially fast in time. The only caveat is that rapid changes in time of u, will lead to rapid changes on M_τ, thereby hindering its efficacy in absorbing trajectories of the BOM equation over finite time. Yet appropriate redefinition of the slow manifold involving history integrals of the fast time scale can compensate the effects of such rapid variations.

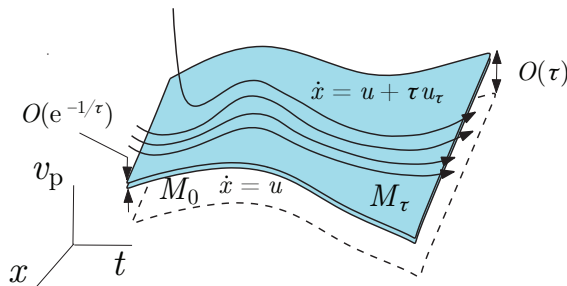
FIGURE 1. Geometry of the BOM dynamics. From [3].

Results from dedicated field [3, 4] and laboratory [5] experiments provided support of the validity of the BOM equation. A critical aspect that contributed to the success of the BOM equation has been its ability to correctly describing windage, as measured by $\alpha(\delta)$. Figure 2 shows theoretical $\alpha(\delta)$ curves along the values
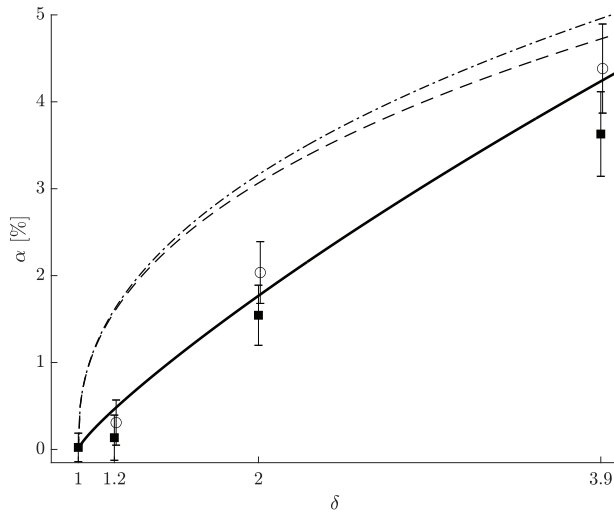
FIGURE 2. As a function of buoyancy, estimated (circles and squares) and theoretical (curves) windage factor. The solid curve corresponds to the BOM prediction and dashed and dot-dashed curves are buoyancy-dependent windage models derived by [7] and [6], respectively. The estimates were made in an air–water flume facility. Figure from [5].

(circles and squares) estimated during laboratory experiments involving the deployment of balloons filled with water up to different levels in an air–stream flume [5]. The BOM equation prediction (solid) is accompanied by other models proposed in the search-and-rescue at sea literature [7, 6]. The BOM's $\alpha(\delta)$ compares very well with the measured data, outperforming other models.

The BOM equation has now been extended to model the motion of elastic networks of floating inertial particles that simulate rafts of *Sargassum* [8], which have inundated the Intra-American Seas, particularly the Caribbean Sea, since early 2010s during the spring and summer months. Further extensions are currently underway to better represent *Sargassum* raft motion. These include the incorporation of nonlinear elastic interactions and changes to the raft geometry due to physiological transformations experienced by *Sargassum* during its life cycle.

REFERENCES

[1] M. R. Maxey, J. J. Riley, *Equation of motion for a small rigid sphere in a nonuniform flow*, Phys. Fluids **26** (1983),883.

[2] F.J. Beron-Vera, M.J. Olascoaga and P. Miron, *Building a Maxey–Riley framework for surface ocean inertial particle dynamics*, Phys. Fluids **31** (2019), 096602.

[3] M.J. Olascoaga, F.J. Beron-Vera, P. Miron, J. Triñanes, N.F. Putman, R. Lumpkin, G.J. Goni, *Observation and quantification of inertial effects on the drift of floating objects at the ocean surface*, Phys. Fluids **32** (2020), 026601.

[4] P. Miron, M.J. Olascoaga, F.J. Beron-Vera, J. Triñanes, N.F. Putman, R. Lumpkin, G.J. Goni, *Clustering of marine-debris-and* Sargassum-*like drifters explained by inertial particle dynamics*, Geophys. Res. Lett. **47** (2020), e2020GL089874.

[5] P. Miron, S. Medina, M.J. Olascoaga, F.J. Beron-Vera, *Laboratory verification of a Maxey–Riley theory for inertial ocean dynamics*, Phys. Fluids **32** (2020), 071703.

[6] O. Nesterov, *Consideration of various aspects in a drift study of MH370 debris*, Ocean Sci. **14** (2018).

[7] J. Rohrs, K. H. Christensen, L. R. Hole, G. Brostrom, M. Drivdal, S. Sundby, *Observation-based evaluation of surface wave effects on currents and trajectory forecasts*, Ocean Dyn. **62** (2012).

[8] F.J. Beron-Vera, P. Miron, *A minimal Maxey–Riley model for the drift of* Sargassum, J. Fluid Mech. **904** (2020), A8.

Network-based analysis of Lagrangian transport and mixing
KATHRIN PADBERG-GEHLE

Lagrangian transport and mixing in fluids have been studied extensively in the last two decades based on different concepts from nonlinear dynamics and ergodic theory. Neglecting molecular diffusion, the motion of passive fluid particles is described by the ordinary differential equation

$$(1) \qquad \dot{\boldsymbol{X}} = \boldsymbol{u}(\boldsymbol{X}, t),$$

where $\boldsymbol{u}(\boldsymbol{X}, t)$ is a sufficiently smooth time-dependent velocity field with state $\boldsymbol{X} \in \mathbb{R}^d$ ($d = 2$ or 3), and time $t \in \mathbb{R}$. Trajectories are obtained as solutions $\boldsymbol{X}(t)$ of this differential equation (1). Coherence can then be described in terms of the manner in which groups of such particle trajectories behave. Our focus is on *probabilistic approaches* that aim to identify full-volume finite-time coherent sets that minimally mix with the surrounding phase space. Originally introduced by means of transfer operators [1], recent research has targeted a data-based identification of coherent sets directly from trajectories.

Suppose we are given N trajectories $\boldsymbol{X}_i(t)$, $i = 1 \ldots N$, at discrete time instances $t \in \mathbb{T} = \{0, \ldots, T\}$, such as obtained by a numerical solution of (1) or by experimental measurements (particle tracking). We construct an undirected network with these particle trajectories serving as network nodes. A link is established between two nodes if the respective trajectories are "close" or "similar". There are different definitions of the distance between two trajectories and thus of "closeness". In [2] an unweighted network was considered with an adjacency matrix $A \in \{0, 1\}^{N \times N}$, where $A_{ij} = 1$ if $\min_{t \in \mathbb{T}} \|\boldsymbol{X}_i(t) - \boldsymbol{X}_j(t)\| < \varepsilon$ for $i \neq j$ and $A_{ij} = 0$ otherwise. Here, $\varepsilon > 0$ is some given threshold. In [3, 4] the number of ε-close encounters was further included as link weights by first constructing instantaneous adjacency matrices $A_t \in \{0, 1\}^{N \times N}$ where $A_{ij,t} = 1$ if $\|\boldsymbol{X}_i(t) - \boldsymbol{X}_j(t)\| < \varepsilon$ for $i \neq j$ and $A_{ij,t} = 0$ otherwise, and then forming the network weight matrix $W = \sum_{t \in \mathbb{T}} A_t$. Here W_{ij} is large if $\boldsymbol{X}_i$ and $\boldsymbol{X}_j$ are close on $\mathbb{T}$ in the sense that they have many ε-close encounters.

To identify coherent sets from the weighted trajectory network, one can make use of spectral clustering with the weight matrix W serving as a similarity matrix

[5, 6]. Moreover, local network measures such as the node degree can be used to identify dynamically distinct regions in the flow [2, 7]. We have applied this framework to geophysical flows (Antarctic polar vortex [2], Agulhas rings [7]), turbulent Rayleigh-Bénard convection flows (e.g. [8, 9]), and recently to a stirred tank reactor from chemical engineering [4].

In [3], the network-based approach was extended to study the evolution of large-scale coherent sets in turbulent flows over long time spans. The evolving cluster approach is based on the preserving cluster membership framework proposed in [11]. Let W_t denote the time-dependent weight matrices that are now computed over a shorter observation window of length $\tau \ll T$ and centered around some time $t \in \mathbb{T}$. As a spectral relaxation to a k-way normalized cut problem [5, 6], for each t, we consider the cost function

$$(2) \qquad \text{Cost}_{\text{NCut}, \, t} = k - \text{Tr} \left[V_t^{\text{T}} \widehat{W}_t V_t \right]$$

Following [11] this is minimized by $V_t \in \mathbb{R}^{N \times k}$, where V_t contains the eigenvectors corresponding to the k largest eigenvalues of the matrix

$$(3) \qquad \widehat{W}_t = \alpha D_t^{-1/2} W_t D_t^{-1/2} + (1 - \alpha) \, V_{t-\Delta t} V_{t-\Delta t}^{\text{T}}.$$

Here $V_{t-\Delta t}$ represent the eigenvectors obtained from the clustering at the previous time instance $t - \Delta t$, where Δt describes the time shift of the observation window. The parameter α regulates the importance of the current connectivity of the graph compared to the previous clustering. To extract k coherent sets from these coordinates in eigenspace, we can make use of a simple k-means clustering or soft clustering by means of a sparse eigenbasis approximation [12].

The evolutionary network approach has been applied to study the long-term evolution of coherent sets in turbulent Rayleigh-Bénard convection [3, 13], including splits and mergers, and their role in the global heat transport. The coherent sets identified by evolutionary clustering are no longer material objects, but particles may leave and enter the time-dependent flow features. A systematic study of these structures, their time scales and their dependence on the parameter α, that weights current and historical costs in (3), is underway. Future work will address the relevant problem of having to deal with very sparse data, measured by sensors or drifters that do not exactly follow the flow.

References

[1] G. Froyland, S. Lloyd, N. Santitissadeekorn, *Coherent sets for nonautonomous dynamical systems*, Physica D **239** (2010) 1527–1541.

[2] K. Padberg-Gehle, C. Schneide, *Network-based study of Lagrangian transport and mixing*, Nonlin. Processes Geophys. **24** (2017) 661–671.

[3] C. Schneide, P. P. Vieweg, J. Schumacher, K. Padberg-Gehle, *Evolutionary clustering of Lagrangian trajectories in turbulent Rayleigh–Bénard convection flows*, Chaos **32** (2022) 013123.

[4] C. Weiland, E. Steuwe, J. Fitschen, M. Hoffmann, M. Schlüter, K. Padberg-Gehle, A. von Kameke, *Computational study of three-dimensional Lagrangian transport and mixing in a stirred tank reactor*, Chemical Engineering Journal Advances **14** (2023) 100448.

[5] J. Shi, J. Malik, *Normalized cuts and image segmentation*, IEEE Trans. Pattern Anal. Mach. Intell. **22** (2000) 888–905.

[6] F. R. Bach, M. I. Jordan, *Learning spectral clustering, with application to speech separation*, J. Mach. Learn. Res.**7** (2006) 1963–2001.

[7] R. Banisch, P. Koltai, K. Padberg-Gehle, *Network measures of mixing*, Chaos **29** (2019) 063125.

[8] C. Schneide, A. Pandey, K. Padberg-Gehle, J. Schumacher, *Probing turbulent superstructures in Rayleigh-Bénard convection by Lagrangian trajectory clusters*, Phys. Rev. Fluids **3** (2018) 113501.

[9] C. Schneide, M. Stahn, A. Pandey, O. Junge, P. Koltai, K. Padberg-Gehle, J. Schumacher, *Lagrangian coherent sets in turbulent Rayleigh-Bénard convection*, Phys. Rev. E **100** (2019) 053103.

[10] P. P. Vieweg, C. Schneide, K. Padberg-Gehle, J. Schumacher, *Lagrangian heat transport in turbulent three-dimensional convection*, Phys. Rev. Fluids **6** (2021) L041501.

[11] Y. Chi, X. Song, D. Zhou, K. Hino, B. L. Tseng, *Evolutionary spectral clustering by incorporating temporal smoothness*, in: Proceedings of the 13th ACM SIGKDD International Conference on Knowledge Discovery and Data Mining (KDD-07), New York, NY, USA, 2007, pp. 153–162.

[12] G. Froyland, C. P. Rock, K. Sakellariou, *Sparse eigenbasis approximation: Multiple feature extraction across spatiotemporal scales with application to coherent set identification*, Commun. Nonlinear Sci. Numer. Simul. **77** (2019) 81–107.

[13] P. P. Vieweg, A. Klünker, J. Schumacher, K. Padberg-Gehle, *Lagrangian studies of coherent sets and heat transport in constant heat flux-driven turbulent Rayleigh-Bénard convection*, under review, arXiv:2304.02984, 2023.

Swell refraction by oceanic currents and multiscale stochastic closures

Valentin Resseguier

(joint work with Erwan Hascoet, Bertrand Chapron)

Swell systems are composed of nearly collimated wave groups traveling rapidly across oceanic basins. Along this propagation, wave groups can be refracted, depending upon strengths of oceanic currents gradients. Small-scale structures of these currents may then become key players but are hardly known, properly simulated or observed by satellite. For this reason, several stochastic closures can be proposed to simulate the dynamics of waves propagating in such a random medium, to eventually facilitate future ensemble-based data assimilation algorithms.

For the submesoscale upper ocean dynamics, $< O(30)$ km, slow-fast time separations [6, 5] – e.g., dynamics under Location Uncertainty (LU) [3] or Stochastic Advection by Lie Transport (SALT) [2] – apply in the wave frame [4]. The wave dynamics can then be described within a Markovian framework.

This is not the case to model unobserved mesoscale, $> O(30)$ km, ocean surface currents. Classical statistical simplifications do not necessarily apply and are often incorrect. To cope with such a difficulty, we consider a new stochastic closure for the wave dynamics. This framework is non-Markovian, multi-scale and still provides low-CPU version to obtain robust results. Considering a kinetic energy spectrum, possibly estimated by self-similarity arguments, a velocity characteristic time $\tau(k)$ can be defined for each wave vector k [1]. From the spatial Fourier transform of a vector of spatio-temporal white noise, $d\widehat{W}(k,t)/dt$, one can thus

generate the Fourier transform of a random velocity field, $\widehat{v'}$, multi-scale in space and time:

$$(1) \qquad d\widehat{v'}(k,t) = -\frac{1}{\tau(k)}\widehat{v'}(k,t)dt + \frac{1}{\sqrt{\tau(k)}} \; ik \times f(k)\|k\|^{-\gamma}d\widehat{W}(k,t),$$

where $\times$ is the cross product, γ is estimated from the self-similarity assumption and f is a high-pass filter. Using stochastic calculus, an analytical formula can then be derived to describe the probability distribution of wave properties (wave vector, frequency and amplitude) at long time. Specifically, it can be shown that the equation of evolution along the ray, $dK/dt = -\nabla(v + v')^T K$, of the wave vector $K = \kappa(\cos\theta, \sin\theta)$ is equivalent to the following pair of equations:

$$(2) \qquad d\ln\kappa(t') = (\alpha^2 - \sin\zeta(t'))dt' + \alpha dB^{(1)}(t'),$$

$$(3) \qquad d\zeta(t') = -\frac{\partial V}{\partial \zeta}(\zeta(t))dt' + (\sqrt{12}\alpha)dB^{(2)}(t'),$$

where $\zeta = 2\theta - \pi/2$, $V(\zeta) = r\zeta - \sin\zeta$ is a potential, r is the ratio between the vorticity and the strain rate of the resolved velocity v, $\alpha^2 = \frac{3}{2}\mathbb{E}\|\nabla(v')^T\|_2^2 dt$ quantifies the amplitude of unresolved submesoscale gradients and $B^{(1)}$ and $B^{(2)}$ are two independent Brownian motions. It is then possible to solve the stationary Fokker-Planck equation for ζ, and to deduce the distribution of the wavenumber growth rate $d\ln\kappa$.

References

[1] U. Frisch (1995), *Turbulence: the legacy of AN Kolmogorov*, Cambridge university press.

[2] D. D. Holm (2015), *Variational principles for stochastic fluid dynamics*, Proceedings of the Royal Society A: Mathematical, Physical and Engineering Sciences **471** (2176), 20140963.

[3] E. Mémin (2014), *Fluid flow dynamics under location uncertainty*, Geophysical & Astrophysical Fluid Dynamics **108** (2), 119-146.

[4] V. Resseguier, E. Hascoët & B. Chapron (2021), *Random ocean swell-rays: a stochastic framework*, Stochastic Transport in Upper Ocean Dynamics Annual Workshop. pp. 259-271, Springer, Cham.

[5] V. Resseguier, L. Li, G. Jouan, P. Dérian, E. Mémin & B. Chapron (2021), *New trends in ensemble forecast strategy: uncertainty quantification for coarse-grid computational fluid dynamics*, Archives of Computational Methods in Engineering **28** (1), 215-261.

[6] V. Resseguier, W. Pan & B. Fox-Kemper (2020), *Data-driven versus self-similar parameterizations for stochastic advection by lie transport and location uncertainty*, Nonlinear Processes in Geophysics **27** (2), 209-234.

Stochastic effects on the movement of small solid particles in fluid flows with application to microplastics in oceanic flows with small-scale turbulence

MASON ROGERS

(joint work with Irina Rypina)

Because of their different sizes, shapes, rigidities, and densities, marine microplastic particles do not follow the same trajectories as fluid parcels. The motion of spherical particles in a flow is described by the Maxey-Riley equations, which depend on the velocity of the fluid in which the particles are immersed. Fluid velocities in the ocean often have a strong small-scale turbulent component which is difficult to observe or model, presenting a challenge to predicting marine microplastic dynamics. To overcome this challenge, we assume that the turbulent velocity acts as a random force on particles and consider a stochastic analogue of the Maxey-Riley equations. By performing a perturbation analysis of the stochastic equations, we obtain a simple and accurate partial differential equation for the number density distribution of an ensemble of plastic particles which handles the uncertainty introduced by unresolved flow features. Numerical test cases demonstrate the agreement between distributions obtained from our reduced model and sample distributions obtained from Monte-Carlo simulations of large numbers of particle trajectories. An additional example integrating our model equation into a high-resolution simulation of the Gulf Stream with the MIT general circulation model begins to explore the interplay between stochastic and inertial effects on particle motion.

REFERENCES

[1] Maxey, M. R., and Riley, J. J., *Equation of motion for a small rigid sphere in a nonuniform flow*, The Physics of Fluids, **26**(4) (1983), 883–889.
[2] Haller, G., and Sapsis, T., *Where do inertial particles go in fluid flows?*, Physica D: Nonlinear Phenomena, **237**(5) (2008), 573–583.
[3] Beron-Vera, F. J., Olascoaga, M. J., and Lumpkin, R., *Inertia-induced accumulation of flotsam in the subtropical gyres*, Geophysical Research Letters, **43**(23) (2016), 12–228.

Analysis of the large-scale flow dynamics in a confined convection flow

JÖRG SCHUMACHER

(joint work with Priyanka Maity, Andreas Bittracher, Péter Koltai)

Complex nonlinear systems typically incorporate orders of magnitude of relevant dynamical scales. Examples at the macroscopic deterministic level are turbulent flows in confined geometries or extended layers with differently ordered large-scale spatial patterns which are visited for longer lasting transients in a long-term evolution. The rapid crossover from one configuration to another is then triggered by fluctuations of secondary flow structures, smaller eddies, shear layers or plumes. This switches can affect the turbulent transport of heat or momentum. The state or phase space of macroscopic flows is infinite– or at least extremely high–dimensional

and typically requires drastic dimensionality reductions to model the observed large-scale dynamics effectively.

Here, we consider the dynamics in a turbulent Rayleigh-Bénard convection flow in a closed cubic cell which is heated from below and cooled from above. The turbulent dynamics in this simple configuration is dominated by multiple long-lived macroscopic circulation states which are visited subsequently by the system. In ref. [1], we identified 6 discrete large-scale circulation states by means of an orientation angle of the circulation roll. We then showed that the long-term dynamics of the flow can be described to a good approximation by a Markov-type hopping process from one of the 6 large-scale circulation states to another. Therefore, we constructed a Markov transition matrix $A \in \mathbb{R}^{6 \times 6}$ and analysed the corresponding eigenvalue spectrum.

In ref. [2], we investigated the short-term transition paths between these subsequent macroscopic system states. This is done by a data-driven learning algorithm that extracts the low-dimensional transition manifold and the related new coordinates, which we term collective variables, in the state space of the complex turbulent flow. We therefore transferred and extended concepts for conformation transitions in stochastic microscopic systems, such as in the dynamics of macromolecules, to a deterministic macroscopic flow. In a first reduction step, a time-lagged independent component analysis was performed to reduce the dimensionality of the data.

Our analysis is based on long-term direct numerical simulation trajectories of turbulent convection in a closed cubic cell at a Prandtl number $Pr = 0.7$ and Rayleigh numbers $Ra = 10^6$ and 10^7 for a time lag of 10^5 convective free-fall time units. All 6 faces of the cube satisfy the no-slip condition. The cube is uniformly heated from below and cooled from above, the side faces are thermally insulated. The simulations resolve vortices and plumes of all physically relevant scales, resulting in an original state space spanned by more than 3.5 million degrees of freedom. The transition dynamics between the large-scale circulation states can be eventually captured by the transition manifold with only two collective variables. This implies a reduction of the data dimension by a factor of more than a million. Our method demonstrates that cessations and subsequent reversals of the large-scale flow are unlikely in the present setup and thus paves the way to the development of efficient reduced-order models of the macroscopic complex nonlinear dynamical system.

REFERENCES

[1] P. Maity, P. Koltai, and J. Schumacher *Large-scale flow in a cubic Rayleigh–Bénard cell: long-term turbulence statistics and Markovianity of macrostate transitions*, Phil. Trans. R. Soc. A **380** (2022), 20210042.

[2] P. Maity, A. Bittracher, P. Koltai, and J. Schumacher *Collective variables between large-scale states in turbulent convection*, Phys. Rev. Research **5** (2023), in press.

Application of Machine Learning to Subgrid-Flux Parametrization of Turbulent Models

ILYA TIMOFEYEV

(joint work with Jeric Alcala)

In this talk, we consider the problem of stochastic parametrization of subgrid fluxes in turbulent models of geophysical flows. First, we present a general framework where we start with a fine-mesh finite-volume discretization of the PDE of interest. We assume that the fine-scale resolution is sufficient to reproduce all physical quantities of interest. Next, we define coarse variables as local averages in physical space and derive equations for coarse variables. However, equations for coarse variables are not closed since the right-hand side of these equations depends on the small-scale (subgrid) variables. Therefore, we seek a parametrization of subgrid fluxes in physical space which is local (involving a small stencil of coarse variables).

First, we compare and contrast the semi-theoretical multiscale approach (joint work with M. Zacharuk, S. I. Dolaptchiev, and U. Achatz) [2, 3, 4] and applications of the Machine Learning (ML) approach [1]. Next, we discuss the ML approach in more detail. In particular, we demonstrate that it is possible to use Generative Adversarial Networks (GANs) to parametrize subgrid fluxes in the context of finite-volume discretizations of turbulent PDEs. We would like to point out that GAN-based parametrizations are ML analogs of stochastic parametrizations since GANs generate samples from a probability distribution of sub-grid fluxes and, thus, are inherently random. We also demonstrate that our subgrid model reproduces stationary properties of turbulent dynamics, such as spectra and temporal correlation functions. We demonstrate the applicability of our approach using two examples - stochastically driven viscous Burger's equation and 1D Shallow water equations. We consider both models in a stationary turbulent regime and demonstrate that subgrid parameterizations are essential for reproducing statistical features such as spectra and correlation functions.

As final remarks, we discuss that the most promising future directions are in combining mathematical multiscale techniques, techniques from numerical analysis, and machine learning. In addition, we also discuss that it is important to develop methods that would allow us to better understand machine learning tools and "extract" useful information such as the structure of subgrid terms.

REFERENCES

[1] J. Alcala and I. Timofeyev, *Subgrid-scale parametrization of unresolved scales in forced Burgers equation using Generative Adversarial Networks (GAN)*, Theor. Comp. Fluid Dyn. **35** (2021), 875–894.

[2] M. Zacharuk, S. I. Dolaptchiev, U. Achatz, I. Timofeyev, *Stochastic subgrid-scale parameterization for one-dimensional shallow water dynamics using stochastic mode reduction*, Q.J.R. Meteorol. Soc. **144(715)** (2018), 1975–1990.

[3] S. I. Dolaptchiev, I. Timofeyev, U. Achatz, *Subgrid-scale closure for the inviscid Burgers-Hopf equation*, Comm. Math Sci. **11(3)** (2013), 757-777.

[4] S. I. Dolaptchiev, U. Achatz, and I. Timofeyev, *Stochastic closure for local averages in the finite-difference discretization of the forced Burgers equation*, Theor. Comput. Fluid Dyn. **27(3-4)** (2013,) 297–317.

Reporter: Anton Kutsenko

Participants

Ekaterina Bagaeva
School of Engineering and Science
Jacobs University Bremen
Campus Ring 1
28759 Bremen
GERMANY

Dr. Sanjeeva Balasuriya
School of Mathematical Sciences
University of Adelaide
Adelaide, SA 5005
AUSTRALIA

Dr. Dwight Barkley
Mathematics Institute
University of Warwick
Gibbet Hill Road
Coventry CV4 7AL
UNITED KINGDOM

**Prof. Dr. Francisco Javier
Beron-Vera**
Department of Atmospheric Sciences
Rosenstiel School of Marine,
Atmospheric, and Earth Science
University of Miami
4600 Rickenbacker Cswy
Miami, FL 33149
UNITED STATES

Dr. Nazmi Burak Budanur
Max Planck Institute for the Physics of
Complex Systems
Nöthnitzer Straße 38
01187 Dresden
GERMANY

Prof. Dr. Oliver Bühler
Center for Atmosphere Ocean Science
Courant Institute of Mathematical
Sciences
New York University
251, Mercer Street
New York, NY 10012-1110
UNITED STATES

Prof. Dr. Michael D. Chekroun
Dept. of Atmosphere and Ocean Science
UCLA
7236 Math Sciences Building
Los Angeles, CA 90095-1565
UNITED STATES

Dr. Jezabel Curbelo
Universitat Politècnica de Catalunya
Department of Mathematics, ETSEIB
Av. Diagonal 647
08028 Barcelona
SPAIN

Michael Dotzel
Woods Hole Oceanographic Institution
PO Department
266 Woods Hole Rd., MS#21
Woods Hole, MA 02540
UNITED STATES

Alex Encinas Bartos
Institute for Mechanical Systems
ETH Zürich
Leonhardstrasse 21
8092 Zürich
SWITZERLAND

Prof. Dr. Jason E. Frank
Mathematical Institute
Universiteit Utrecht
Budapestlaan 6
3584 CD Utrecht
NETHERLANDS

Prof. Dr. Christian Franzke
IBS Center for Climate Physics
Busandaehak-ro 63beon-gil 2
46241 Busan
KOREA, REPUBLIC OF

Prof. Dr. Gary Froyland
School of Mathematics and Statistics
University of New South Wales
Sydney, NSW 2052
AUSTRALIA

Dr. Anna Geyer
Delft Institute of Applied Mathematics
and Computer Science
Delft University of Technology
Mekelweg 4
2628 XE Delft
NETHERLANDS

Prof. Dr. Georg A. Gottwald
School of Mathematics and Statistics
The University of Sydney
Sydney, NSW 2206
AUSTRALIA

Prof. Dr. John Harlim
Department of Mathematics
Pennsylvania State University
University Park, PA 16802
UNITED STATES

Dr. Sabine Hittmeir
Fakultät für Mathematik
Universität Wien
Oskar-Morgenstern-Platz 1
1090 Wien
AUSTRIA

Prof. Dr. Darryl D. Holm
Department of Mathematics
Imperial College London
Huxley Building
London SW7 2AZ
UNITED KINGDOM

Paul Holst
Fachbereich 3 –
Mathematik und Informatik
Universität Bremen
Postfach 33 04 40
28334 Bremen
GERMANY

Dr. Yu Huang
Technical University of Munich
TUM School of Engineering and Design
Lise-Meitner-Straße 9
85521 Ottobrunn
GERMANY

Prof. Dr. Helga Huntley
Rowan University
Department of Mathematics
201 Mullica Hill Road
Glassboro, NJ 08028
UNITED STATES

Dr. Delia Ionescu-Kruse
Institute of Mathematics
"Simion Stoilow"
of the Romanian Academy of Sciences
P.O. Box 1-764
014700 Bucharest
ROMANIA

Dr. Janin Jäger
Mathematisch-Geographische Fakultät
Kath. Universität Eichstätt
Ostenstr. 26-28
85072 Eichstätt
GERMANY

Prof. Dr. Oliver Junge
Department of Mathematics
Technical University of Munich
Boltzmannstr. 3
85748 Garching bei München
GERMANY

Dr. Stephan Juricke
School of Engineering and Science
Jacobs University Bremen
28725 Bremen
GERMANY

Prof. Dr. Marc Keßeböhmer
Fachbereich 3
Mathematik und Informatik
Universität Bremen
Bibliothekstr. 1
28359 Bremen
GERMANY

Prof. Dr. Rupert Klein
Fachbereich Mathematik und Informatik
Freie Universität Berlin
Arnimallee 6
14195 Berlin
GERMANY

Prof. Dr. Edgar Knobloch
Department of Physics
University of California, Berkeley
376 Le Conte Hall
Berkeley, CA 94720-7300
UNITED STATES

Dr. Anton Kutsenko
Katholische Universität
Eichstätt-Ingolstadt
Mathematisches Institut für Maschinelles
Lernen und Data Science
Auf der Schanz 49
85049 Ingolstadt
GERMANY

Prof. Dr. Ana Maria Mancho
Instituto de Ciencias Matematicas, CSIC
Campus Cantoblanco, UAM
Nicolas Cabrera, 13-15
28049 Madrid
SPAIN

Jamie Meacham
Imperial College London
Department of Mathematics
Huxley Building
180 Queen's Gate
London SW7 2AZ
UNITED KINGDOM

Prof. Dr. Jim Meiss
Dept. of Applied Mathematics
University of Colorado at Boulder
Campus Box 526
Boulder, CO 80309-0526
UNITED STATES

David Meyer
Institut für Numerische und
Angewandte Mathematik
Universität Münster
Orleans-Ring 10
48149 Münster
GERMANY

Dr. Philippe Miron
Center for Ocean-Atmospheric
Prediction Studies (COAPS)
Florida State University
Building A, Suite 292
2000 Levy Avenue
Tallahassee, FL 32306-2741
UNITED STATES

Dr. Florian Noethen
Department Mathematik
Universität Hamburg
Bundesstr. 55
20146 Hamburg
GERMANY

Prof. Dr. Josefina Olascoaga
University of Miami
Rosenstiel School of Marine and
Atmospheric Science
4600 Rickenbacker Causeway
Miami, FL 33149
UNITED STATES

Prof. Dr. Marcel Oliver
Chair of Applied Mathematics
Mathematical Institute for Machine
Learning and Data Science
KU Eichstätt-Ingolstadt
Auf der Schanz 49
85049 Ingolstadt
GERMANY

Dr. Ivan Ovsyannikov
MARUM
Universität Bremen
Fachbereich 3
Bibliothekstraße 5
28359 Bremen
GERMANY

Prof. Dr. Kathrin Padberg-Gehle
Institut für Mathematik
und ihre Didaktik
Leuphana Universität Lüneburg
Universitätsallee 1
21335 Lüneburg
GERMANY

Prof. Dr. Jens Rademacher
Fakultät für Mathematik, Informatik
und Naturwissenschaften
Fachbereich Mathematik
Universität Hamburg
Bundesstr. 55
20146 Hamburg
GERMANY

Dr. Valentin Resseguier
SCALIAN DS & INRAE
Espace Nobel – 2 Allée de Becquerel
35700 Rennes
FRANCE

Mason Rogers
Woods Hole Oceanographic Institution
PO Department
266 Woods Hole Rd., MS#21
Woods Hole, MA 02540
UNITED STATES

Prof. Dr. Irina Rypina
Woods Hole Oceanographic Institution
266 Woods Hole Rd., MS #21
Woods Hole, MA 02543
UNITED STATES

Susmit Subhransu Satpathy
IBS Center for Climate Physics
Busandaehak-ro 63beon-gil 2
46241 Busan
KOREA, REPUBLIC OF

Prof. Dr. Jörg Schumacher
Institut für Thermo- und Fluiddynamik
Technische Universität Ilmenau
Postfach 100565
98684 Ilmenau
GERMANY

Dr. Radomyra Shevchenko
Max Planck Institute for Meteorology
Bundesstr. 53
20146 Hamburg
GERMANY

Prof. Dr. Jean-Luc Thiffeault
Department of Mathematics
University of Wisconsin-Madison
480 Lincoln Drive
Madison, WI 53706-1685
UNITED STATES

Prof. Dr. Ilya Timofeyev
Department of Mathematics
University of Houston
4800 Calhoun Rd.
Houston, TX 77204-3476
UNITED STATES

Marc Aurele Tiofack Kenfack
Katholische Universität
Eichstätt-Ingolstadt
Mathematisches Institut für Maschinelles
Lernen und Data Science
Auf der Schanz 49
85049 Ingolstadt
GERMANY

Prof. Dr. Beth Wingate
Department of Mathematics
and Statistics
University of Exeter
Harrison Building
North Park Road
Exeter EX4 4QF
UNITED KINGDOM

Prof. Dr. Lennaert van Veen
Ontario Tech
2000 Simcoe Street North
Oshawa L1H 7K4
CANADA

Dr. Caroline Wormell
Mathematical Sciences Institute
Australian National University
Canberra 2601
AUSTRALIA